Journal of Geodesy (2018) 92:1199–1217
https://doi.org/10.1007/s00190-018-1146-y

ORIGINAL ARTICLE

Estimation of satellite position, clock and phase bias corrections

Patrick Henkel[1] · **Dimitrios Psychas**[1] · **Christoph Günther**[1,2] · **Urs Hugentobler**[1]

Received: 8 November 2017 / Accepted: 12 April 2018 / Published online: 2 May 2018

Abstract

Precise point positioning with integer ambiguity resolution requires precise knowledge of satellite position, clock and phase bias corrections. In this paper, a method for the estimation of these parameters with a global network of reference stations is presented. The method processes *uncombined* and *undifferenced* measurements of an *arbitrary* number of frequencies such that the obtained satellite position, clock and bias corrections can be used for any type of differenced and/or combined measurements. We perform a clustering of reference stations. The clustering enables a common satellite visibility within each cluster and an efficient fixing of the double difference ambiguities within each cluster. Additionally, the double difference ambiguities between the reference stations of different clusters are fixed. We use an integer decorrelation for ambiguity fixing in dense *global* networks. The performance of the proposed method is analysed with both simulated Galileo measurements on E1 and E5a and real GPS measurements of the IGS network. We defined 16 clusters and obtained satellite position, clock and phase bias corrections with a precision of better than 2 cm.

Keywords Network solution · Satellite phase biases · Satellite position and clock corrections · Ambiguity fixing

1 Introduction

Precise point positioning (PPP) is becoming attractive since the user does not need raw measurements from a reference station. Zumberge et al. (1997) introduced PPP using precise orbits and clocks obtained from a large network of reference stations. Dong and Bock (1989) performed a global positioning system network analysis with phase ambiguity resolution and applied it to crustal deformation studies in California.

Kouba and Héroux (2001) describe PPP including a precise modelling of satellite antenna offsets, phase wind-up corrections, solid earth tides, ocean loading and earth rotation parameters. They also assessed the performance of PPP using IGS (International GNSS Service) products. Precise satellite orbit and clock information can be obtained, e.g. by the bernese GNSS software as described by Dach et al. (2007).

Precise knowledge of satellite phase biases is required for PPP with integer ambiguity fixing. Gabor and Nerem (2002) and Ge et al. (2008) used the Melbourne Wübbena combination and the ionosphere-free phase combination to determine satellite–satellite *single-difference* phase biases. The estimation is performed in two steps, i.e. a first step for the widelane ambiguity fixing, and a subsequent step for fixing the narrowlane ambiguities. Ge et al. (2008) applied the Melbourne Wübbena combination and the ionosphere-free phase combination to satellite–satellite single-difference measurements of 450 IGS (International GNSS Service) stations. The estimated phase biases varied by only 0.4 cycles per day for some GPS satellites, and a reliable narrow ambiguity fixing was demonstrated. Initial work on GPS network design with undifferenced GPS observations was made already by Lindlohr and Wells (1985).

Integer ambiguity resolution with undifferenced GPS phase measurements was performed by Laurichesse and Mercier (2007), Collins (2008) and Collins et al. (2010) and applied to orbit determination in Laurichesse et al. (2009). Real-time PPP with undifferenced integer ambiguity resolution with experimental results was demonstrated in Laurichesse et al. (2010). *Undifferenced* satellite phase clocks, station clocks, satellite differential code/phase bias, station differential code/ phase biases, station coordinate

✉ Patrick Henkel
patrick.henkel@tum.de

Christoph Günther
christoph.guenther@dlr.de

1 Technische Universität München, Munich, Germany

2 German Aerospace Center (DLR), Oberpfaffenhofen, Germany

corrections, satellite orbit corrections and ambiguities are estimated in a Kalman filter. The same combinations as in Ge et al. (2008) were used, but undifferenced measurements were processed. Laurichesse et al. (2010) analysed also the evolution of the narrowlane pseudorange minus phase biases over the whole year 2008 for all GPS satellites. They distinguished between blocks IIA and IIR satellites and observed a drift of only 3 narrowlane cycles per year. Wen et al. (2011) proposed to estimate the undifferenced satellite phase biases, non-dispersive geometry correction terms including their time derivatives, slant ionospheric delays and carrier phase ambiguities in a Kalman filter. The ambiguity fixing was triggered based on the stability of the float solution and the statistics of the Kalman filter. The method was applied to the regional network of SAPOS reference stations in Germany.

More recent work on PPP includes triple-frequency GPS precise point positioning with rapid ambiguity resolution of Geng and Bock (2013), the analysis on the estimability of parameters in undifferenced, uncombined GNSS networks of Odijk et al. (2016), and the performance analysis of real-time precise point positioning using IGS real-time service of Elsobeiey and Al-Harbi (2016).

Carrier phase integer ambiguity fixing is essential for precise satellite phase bias estimation. Blewitt (1989) proposed a sequential ambiguity fixing, which partially exploits the correlation between float ambiguities. The correlation was obtained from a triangular decomposition of the float ambiguity covariance matrix. Teunissen (1995) developed the famous Least-squares AMBiguity Decorrelation Adjustment (LAMBDA) method to solve the integer least-squares problem. The LAMBDA method includes an integer decorrelation and a sequential tree search to find the integer ambiguities which minimize the sum of squared ambiguity residuals. Teunissen (1998) provides an expression for the success rate of integer bootstrapping based on the cumulative Gaussian distribution. Brack et al. (2014) proposed a *sequential* best-integer equivariant (BIE) estimator for high-dimensional integer ambiguity fixing. The authors performed n one-dimensional searches instead of one n-dimensional search, which is much more efficient. The sequential BIE was used for satellite phase bias estimation with 20 reference stations. Henkel et al. (2016) developed an ambiguity transformation for GLONASS double difference carrier phase measurements to enable integer ambiguity fixing for FDMA-modulated signals. The transformation is used for joint ambiguity fixing of GPS and GLONASS.

The estimation of satellite position, clock and phase bias corrections with today's orbit determination software packages (e.g. GIPSY, bernese GNSS software) has several weaknesses: first, the clustering of the receivers and the parameter mapping have not yet been optimized from a global perspective of ambiguity fixing. Therefore, the integer property of ambiguities has not yet been fully exploited. Moreover, the ambiguity fixing for global network solutions has not yet been performed with integer decorrelation despite the strong correlations between ambiguities.

In this paper, we provide a method for the estimation of satellite phase biases, satellite position and clock corrections with undifferenced and uncombined measurements that overcomes the previous shortcomings by an optimized clustering, an optimized parameter mapping and an ambiguity fixing with integer decorrelation. The method uses a global network of reference stations and consists of three steps as shown in Fig. 1.

The first step includes the optimization of the clusters based on the coordinates of the reference stations. In the second step, satellite position, clock and phase bias corrections are estimated with an individual Kalman filter and ambiguity fixing for each cluster. The third step includes the combination of the individual cluster solutions by least-squares estimation and ambiguity fixing. Thereby, one cluster has to serve as reference cluster, which we highlighted in orange. The Kalman filter and single-epoch least-squares estimation process the measurements epoch by epoch, i.e. the method can be used for both real-time processing and post-processing.

We perform a clustering of the global receiver network for the following reasons:

- selection of *common* reference satellite and *common* reference receiver for all measurements is only feasible with regional coverage
- common visibility at reference receiver and any other receiver within a cluster enables expression of real-valued undifferenced ambiguity/phase biases of *any receiver* in terms of real-valued undifferenced ambiguity/phase biases of *reference receiver* and of double difference integer ambiguities
- reduced dimensions of measurements and states within each cluster enables integer ambiguity *decorrelation* and *fixing*
- selection of a receiver-independent reference satellite enables a *transformation* instead of a *re-estimation* of receiver and satellite clock offsets, receiver phase biases and double difference integer ambiguities in case of *changing reference satellite*

The next section describes the criteria for cluster optimization and the mapping of receivers to clusters.

2 Cluster optimization

In this section, we describe the cluster optimization, i.e. the determination of the optimized number of clusters and their

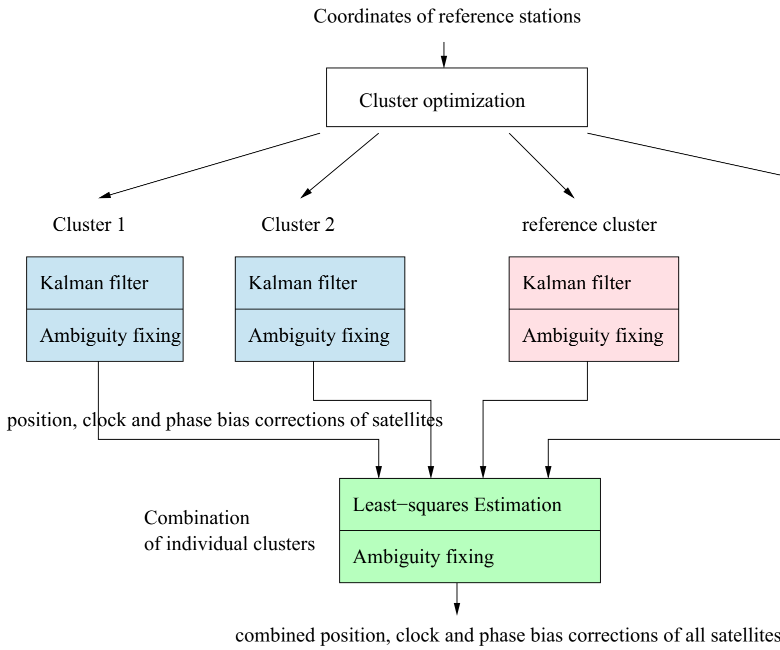

Fig. 1 Functional diagram for the estimation of satellite position, clock and phase bias corrections with clustering of the receivers and integer ambiguity fixing

regions. We consider only non-overlapping clusters, i.e. each receiver is mapped to only one cluster. A large number of receivers per cluster is attractive since it enables a more accurate estimation of the respective satellite position, clock and bias corrections. Moreover, short distances between the receivers enable a fast fixing of the carrier phase ambiguities. A second objective of the cluster optimization is to have a large number of commonly visible satellites within a cluster. This common satellite visibility is desired since only double difference ambiguities can be fixed to integers within each cluster. This second objective limits the size of each cluster. Moreover, two additional constraints need to be considered: first, there is a minimum number of receivers per cluster to obtain a full-rank system of equations. Secondly, a minimum distance of the receivers within each cluster is required to enable a separation of satellite position and clock offset corrections and tropospheric zenith delays.

The minimum number of receivers per cluster follows from the number of measurements and the number of unknowns related to one particular satellite: we use the code and carrier phase measurements of R receivers on M frequencies leading to $2RM$ measurements per epoch. The satellite position, clock offset, phase and code bias corrections and ionospheric delays lead to a set of $4 + M + (M - 2) + R$ unknown parameters per satellite and per epoch. Moreover, there are MR unknown ambiguities per satellite. Thus, the minimum number of receivers for measurements of N_{ep} epochs is given by $R \geq \big((4 + M + (M - 2))N_{\text{ep}}\big) / \big(2MN_{\text{ep}} - N_{\text{ep}} - M\big)$. This leads to a minimum of 6 receivers for dual-frequency single- epoch measurements and to a minimum of 4 receivers for triple-frequency single-epoch measurements. These constraints are relaxed to some extent by the use of prior information on the satellite position and clock offsets. Nevertheless, we impose a constraint of at least 4 receivers per cluster to reduce the dependency on the prior information.

Each cluster is defined by its reference receiver $\text{ref}(c)$, which is located in the middle of the cluster. The selection of the reference receivers is part of the global cluster optimization. In principle, any receiver $r \in \{1, \ldots, R\}$ can serve as reference receiver.

A cluster includes all receivers that are closer to the cluster's reference receiver than to the reference receiver of any other cluster. This unique mapping of each receiver $r \in \{1, \ldots, R\}$ to one cluster $c \in \{1, \ldots, C\}$ is denoted by:

$$r \rightarrow c_{\text{opt}} = \arg\min_{c} \left\| \mathbf{x}_r - \mathbf{x}_{\text{ref}(c)} \right\|^2, \tag{1}$$

with $\mathbf{x}_r$ being the position of the rth receiver and $\mathbf{x}_{\text{ref}(c)}$ being the position of the reference receiver of cluster c.

The cluster optimization needs to consider the contrary objectives of maximizing the number of receivers per cluster and maximizing the common satellite visibility. Both objectives are addressed in the *measurement density* defined as

$$\rho^c(\text{ref}(c)) = \frac{1}{A^c} \sum_{r=1}^{R^c} K^c_{r,\text{ref}(c)}, \tag{2}$$

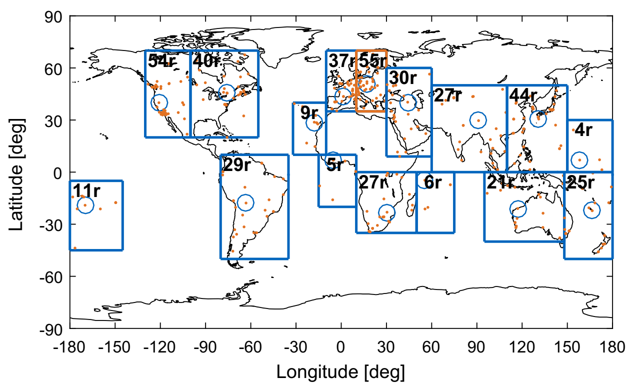

Fig. 2 Global network of IGS stations, split into 16 clusters centred around the densest areas of reference stations. The reference receiver of each cluster is marked with a blue circle. The number of receivers per cluster is provided in the upper left of corner of each cluster

with the cluster's area A^c, the number of receivers R^c of the cluster, and the number of jointly visible satellites $K^c_{r,\mathrm{ref}(c)}$ at receiver r and at the reference receiver. The normalization with the area penalizes for receivers that are far from the reference receiver and, thus, have only a reduced number of jointly visible satellites. The mapping of receivers to clusters needs to be optimized from a global perspective. We determine the number of clusters and the reference receiver of each cluster by maximizing the sum of measurement densities from all clusters:

$$\max_{C}\left(\max_{\mathrm{ref}(1),\ldots,\mathrm{ref}(C)} \sum_{c=1}^{C} \rho^c\left(\mathrm{ref}(c)\right)\right)$$
$$\text{s.t.}\quad R^c \geq R^c_{\min}\ \forall\, c \quad \wedge \quad A^c \geq A^c_{\min}\ \forall\, c, \tag{3}$$

with the constraints on the minimum number of receivers $R^c_{\min}$ and minimum area $A^c_{\min}$ for each cluster.

The input for the cluster optimization is the coordinates of the reference stations. We consider the 424 stations of the International GNSS Service [see Dow et al. (2009)] and impose a minimum of 4 receivers per cluster, and a minimum length of 1000 km in both lateral and longitudinal directions for each cluster.

Figure 2 shows the optimized map with the locations of the 424 IGS stations. We obtained 16 clusters centred around the densest areas of reference stations. The reference receiver of each cluster is marked with a blue circle. The number of receivers per cluster is provided in the upper left of corner of each cluster. The Central European Cluster with 55 reference station is selected as reference cluster (highlighted with orange box) due to the maximum number of receivers within this cluster. A few stations located in Antarctica and some Pacific islands (e.g. Galapagos) were disregarded due the sparsity of these areas.

3 Measurement model

In this section, the measurement model for *uncombined* and *undifferenced* carrier phase and pseudorange observations is provided. The carrier phase measured at receiver $r \in \{1,\ldots,R\}$ on frequency $m = \{1,\ldots,M\}$ of satellite $k = \{1,\ldots,K\}$ is modelled as

$$\begin{aligned}\lambda_m \varphi^k_{r,m} = {} & (\mathbf{e}^k_r)^{\mathrm{T}}\left((\mathbf{x}_r + \Delta\mathbf{x}_{\mathrm{ET},r}) - (\hat{\mathbf{x}}^k_r + \Delta\mathbf{x}^k)\right)\\ & + c\left(\delta\tau_r - \left(\delta\hat{\tau}^k + \Delta\delta\tau^k\right)\right)\\ & + m_{\mathrm{T}}(E^k_r)T_{\mathrm{z},r} - q^2_{1m} I^k_{r,1}\\ & + \lambda_m\left(\Delta\varphi^k_{\mathrm{PW},r} + \Delta\varphi^k_{\mathrm{PCO},r,m} + \Delta\varphi^k_{\mathrm{PCV},r,m}\right)\\ & + \lambda_m\left(N^k_{r,m} + \beta_{r,m} - \beta^k_m\right) + \varepsilon^k_{r,m} \quad \forall\, r, m, k,\end{aligned} \tag{4}$$

with the wavelength λ_m, the carrier phase measurement $\varphi^k_{r,m}$ as provided by the phase locked loop in units of cycles, the line of sight vector $\mathbf{e}^k_r$ pointing from the satellite to the receiver, the receiver position $\mathbf{x}_r$, the Earth tides $\Delta\mathbf{x}_{\mathrm{ET},r}$, the satellite position estimate $\hat{\mathbf{x}}^k_r$ at the time of signal transmission (depending on the signal propagation time and, therefore, on the receiver's position) obtained, e.g. from the broadcast orbits, the correction $\Delta\mathbf{x}^k$ of the satellite position estimate, the speed of light c, the receiver clock offset $\delta\tau_r$, the satellite clock offset estimate $\delta\hat{\tau}^k$ as provided, e.g. by the broadcast clocks, the satellite clock correction $\Delta\delta\tau^k$, the tropospheric mapping function m_{T} depending on the elevation angle E^k_r, the tropospheric zenith delay $T_{\mathrm{z},r}$, the ratio of frequencies $q_{1m} = f_1/f_m$, the ionospheric slant delay $I^k_{r,1}$ on f_1, the phase wind-up $\Delta\varphi^k_{\mathrm{PW},r}$, the antenna phase centre offset $\Delta\varphi^k_{\mathrm{PCO},r,m}$ and variation $\Delta\varphi^k_{\mathrm{PCV},r,m}$, the integer ambiguity $N^k_{r,m}$, the receiver and satellite phase biases $\beta_{r,m}$ and β^k_m in units of cycles and phase noise $\varepsilon^k_{r,m}$. The satellite position correction $\Delta\mathbf{x}^k$ is modelled in the RIC (radial, in-track, cross-track) frame and subsequently transformed to the ECEF (Earth-Centred Earth-Fixed) coordinate frame based on the satellite's attitude.

The pseudoranges are modelled similarly as

$$\begin{aligned}\rho^k_{r,m} = {} & (\mathbf{e}^k_r)^{\mathrm{T}}\left((\mathbf{x}_r + \Delta\mathbf{x}_{\mathrm{ET},r}) - (\hat{\mathbf{x}}^k_r + \Delta\mathbf{x}^k)\right)\\ & + c\left(\delta\tau_r - \left(\delta\hat{\tau}^k + \Delta\delta\tau^k\right)\right)\\ & + m_{\mathrm{T}}(E^k_r)T_{\mathrm{z},r} + q^2_{1m} I^k_{r,1}\\ & + \lambda_m\left(\Delta\varphi^k_{\mathrm{PCO},r,m} + \Delta\varphi^k_{\mathrm{PCV},r,m}\right)\\ & + b_{r,m} - b^k_m + \Delta\rho^k_{\mathrm{MP}_{r,m}} + \eta^k_{r,m} \quad \forall\, r, m, k,\end{aligned} \tag{5}$$

with the code biases $b_{r,m}$ and b^k_m, the pseudorange multipath $\Delta\rho^k_{\mathrm{MP}_{r,m}}$ and the pseudorange noise $\eta^k_{r,m}$.

The raw carrier phases are corrected for the known parameters of the receiver's position, the Earth tides, the estimated satellite position and clock offset, the phase wind-up, the phase centre offset and variation:

$$\lambda_m \tilde{\varphi}^k_{r,m} = \lambda_m \varphi^k_{r,m} - (\mathbf{e}^k_r)^{\mathrm{T}}((\mathbf{x}_r + \Delta\mathbf{x}_{\mathrm{ET},r}) - \hat{\mathbf{x}}^k_r) + c\delta\hat{\tau}^k - \lambda_m \left(\Delta\varphi^k_{\mathrm{PW},r} + \Delta\varphi^k_{\mathrm{PCO},r,m} + \Delta\varphi^k_{\mathrm{PCV},r,m}\right). \quad (6)$$

Similarly, the pseudoranges are corrected as:

$$\tilde{\rho}^k_{r,m} = \rho^k_{r,m} - (\mathbf{e}^k_r)^{\mathrm{T}}((\mathbf{x}_r + \Delta\mathbf{x}_{\mathrm{ET},r}) - \hat{\mathbf{x}}^k_r) + c\delta\hat{\tau}^k - \lambda_m \left(\Delta\varphi^k_{\mathrm{PCO},r,m} + \Delta\varphi^k_{\mathrm{PCV},r,m}\right). \quad (7)$$

4 Parameter mapping

In this section, we introduce a parameter mapping that (a) combines some of the above parameters in order to obtain a full-rank system of observation equations and (b) combines ambiguities mainly with ambiguities to preserve their integer property. The theoretical framework for the parameter mapping is given by the S-system theory of Baarda (1973), which has been used by Odijk et al. (2016) to determine the estimable parameters in GNSS networks using undifferenced and uncombined measurements. The mapping requires the selection of a reference receiver and reference satellite being denoted by the lower/upper index ref. As the reference receiver and reference satellite are cluster dependent, we introduce the index $c = \{1, \ldots, C\}$ to denote all cluster-dependent parameters.

The rank defect of the absolute clock offset estimation is prevented by mapping the satellite clock offset of the reference satellite ref (c) of cluster c to the receiver clock offset, i.e.

$$\delta\tilde{\tau}_{r,c} := \delta\tau_r - \Delta\delta\tau^{\mathrm{ref}(c)} \quad \forall\, r, c. \quad (8)$$

The clock offsets of the other satellites are adjusted, respectively:

$$\Delta\delta\tilde{\tau}^k_c := \Delta\delta\tau^k - \Delta\delta\tau^{\mathrm{ref}(c)} \quad \forall\, k, c. \quad (9)$$

The clock offset and ionospheric delay are two parameters per satellite and, therefore, can absorb the code biases $b_{r,m}$ and b^k_m of the first two frequencies:

$$\begin{pmatrix} b_{r,1} - b^k_1 \\ b_{r,2} - b^k_2 \\ b_{r,3} - b^k_3 \\ \vdots \\ b_{r,M} - b^k_M \end{pmatrix} = \Lambda \begin{pmatrix} b_{\delta\tau_r} - b_{\Delta\delta\tau^k} \\ b_{I^k_{r,1}} \\ \tilde{b}_{r,3} - \tilde{b}^k_3 \\ \vdots \\ \tilde{b}_{r,M} - \tilde{b}^k_M \end{pmatrix}, \quad (10)$$

where $b_{\delta\tau_r}$, $b_{\Delta\delta\tau^k}$ and $b_{I^k_{r,1}}$ decribe the biases of the receiver clock offset, satellite clock offset and ionospheric delay due to the absorption of code biases. The mapping matrix Λ is given by

$$\Lambda = \begin{pmatrix} 1 & 1 & 0 \cdots 0 \\ 1 & q^2_{12} & 0 \cdots 0 \\ 1 & q^2_{13} & 1 \quad\;\; 0 \\ \vdots & \vdots & \ddots \\ 1 & q^2_{1M} & 0 \quad\;\; 1 \end{pmatrix} \quad (11)$$

Solving for the biases of the clock offsets and ionospheric delays gives:

$$\begin{pmatrix} b_{\delta\tau_r} - b_{\Delta\delta\tau^k} \\ b_{I^k_{r,1}} \\ \tilde{b}_{r,3} - \tilde{b}^k_3 \\ \vdots \\ \tilde{b}_{r,M} - \tilde{b}^k_M \end{pmatrix} = \Lambda^{-1} \cdot \begin{pmatrix} b_{r,1} - b^k_1 \\ b_{r,2} - b^k_2 \\ b_{r,3} - b^k_3 \\ \vdots \\ b_{r,M} - b^k_M \end{pmatrix}. \quad (12)$$

The receiver clock offset of Eq. (8) is extended to:

$$c\delta\tilde{\tilde{\tau}}_{r,c} := c\left(\delta\tau_r - \Delta\delta\tau^{\mathrm{ref}(c)}\right) + \sum_{m=1}^{M} \gamma_{1m} \cdot (b_{r,m} - b^{\mathrm{ref}(c)}_m), \quad (13)$$

with γ_{1m} being the element of the first row and mth column of Λ^{-1}. The satellite clock offsets of Eq. (9) are adjusted, respectively, i.e.

$$c\Delta\delta\tilde{\tilde{\tau}}^{k,c} := c\left(\Delta\delta\tau^k - \Delta\delta\tau^{\mathrm{ref}(c)}\right) + \sum_{m=1}^{M} \gamma_{1m} \cdot (b^k_m - b^{\mathrm{ref}(c)}_m). \quad (14)$$

The slant ionospheric delay is adjusted similarly as:

$$\tilde{I}^k_{r,1} := I^k_{r,1} + \sum_{m=1}^{M} \gamma_{2m} \cdot (b_{r,m} - b^k_m), \quad (15)$$

with γ_{2m} denoting the element of the second row and mth column of Λ^{-1}.

The estimation of an individual receiver phase bias for each receiver, of an individual satellite phase bias for each satellite, and of an individual integer ambiguity for each link is not feasible due to a rank deficiency. We perform the following parameter mappings to overcome the rank defect:

– mapping of the phase bias of the reference receiver to the satellite phase biases

– mapping of the ambiguities of the reference receiver to the satellite phase biases
– mapping of the ambiguities of the reference satellite to the receiver phase biases

Additionally, the phase biases have to be corrected for the code biases being mapped into the clock offsets and ionospheric delay. Thus, the receiver phase bias with lumped code biases and ambiguities of reference receiver and satellite is given by

$$\begin{aligned}\lambda_m \tilde{\beta}_{r,c,m} := \lambda_m \left(\beta_{r,m} - \beta_{\mathrm{ref}(c),m}\right) \\ - \sum_{m=1}^{M} \gamma_{1m} \cdot (b_{r,m} - b_{\mathrm{ref}(c),m}) \\ + \sum_{m=1}^{M} q_{1m}^2 \cdot \gamma_{2m} \cdot (b_{r,m} - b_{\mathrm{ref}(c),m}) \\ + \lambda_m \left(N_{r,m}^{\mathrm{ref}(c)} - N_{\mathrm{ref}(c),m}^{\mathrm{ref}(c)}\right) \quad \forall\, r, c, m. \qquad (16)\end{aligned}$$

The satellite phase bias is adjusted, respectively, i.e.

$$\begin{aligned}\lambda_m \tilde{\beta}_m^{k,c} := \lambda_m \left(\beta_m^k - \beta_{\mathrm{ref}(c),m}\right) - \sum_{m=1}^{M} \gamma_{1m} \cdot (b_m^k - b_{\mathrm{ref}(c),m}) \\ + \sum_{m=1}^{M} q_{1m}^2 \cdot \gamma_{2m} \cdot (b_m^k - b_{\mathrm{ref}(c),m}) \\ - \lambda_m N_{\mathrm{ref}(c),m}^k \quad \forall\, k, c, m. \qquad (17)\end{aligned}$$

Each integer ambiguity is related to the integer ambiguity of the reference receiver and reference satellite, which results in the well-known double difference integer ambiguity:

$$\tilde{N}_{r,c,m}^{\bar{k}_r} := (N_{r,m}^{\bar{k}_r} - N_{r,m}^{\mathrm{ref}(c)}) - (N_{\mathrm{ref}(c),m}^{\bar{k}_r} - N_{\mathrm{ref}(c),m}^{\mathrm{ref}(c)}) \quad \forall r, c, \bar{k}, \qquad (18)$$

where $\bar{k}_r \in \{1, \ldots, K_r\}$ denotes the visible satellites at receiver r.

The corrected undifferenced carrier phase and pseudorange measurements of Eqs. (6) and (7) are expressed in terms of the reduced parameter set, i.e. as a function of the satellite position correction Δx^k, the zenith tropospheric delay $T_{\mathrm{z},r}$, the slant ionospheric delay $\tilde{I}_{r,1}^k$ with mapped code biases of Eq. (15), the receiver and satellite clock offset corrections $\delta\tilde{\tilde{\tau}}_{r,c}$ and $\Delta\delta\tilde{\tilde{\tau}}^{k,c}$ with mapped code biases of Eqs. (13) and (14), the receiver and satellite phase bias corrections $\tilde{\beta}_{r,c,m}$ and $\tilde{\beta}_m^{k,c}$ with mapped phase biases, code biases and ambiguities of Eqs. (16) and (17), and the double difference integer ambiguities $\tilde{N}_{r,c,m}^k$ of Eq. (18). The resulting full-rank observation equations are provided in Eqs. (19) and (20). Some parameters vanish and are not estimated for $r = \mathrm{ref}$ or $k = \mathrm{ref}$ since the respective parameters were mapped to other parameters.

$$\begin{aligned}\lambda_m \tilde{\varphi}_{r,m}^k &= (\mathbf{e}_r^k)^{\mathrm{T}}(-\Delta \mathbf{x}^k) + m_{\mathrm{T}}(E_r^k) T_{\mathrm{z},r} - q_{1m}^2 \tilde{I}_{r,1}^k \\ &+ \begin{cases} c(\delta\tilde{\tilde{\tau}}_{r,c} - \Delta\delta\tilde{\tilde{\tau}}^{k,c}) + \lambda_m(\tilde{\beta}_{r,c,m} - \tilde{\beta}_m^{k,c} + \tilde{N}_{r,c,m}^k) + \varepsilon_{r,m}^k & r \neq \mathrm{ref}, k \neq \mathrm{ref} \\ c\delta\tilde{\tilde{\tau}}_{r,c} + \lambda_m(\tilde{\beta}_{r,c,m} - \tilde{\beta}_m^{k,c}) + \varepsilon_{r,m}^k & r \neq \mathrm{ref}, k = \mathrm{ref} \\ c(\delta\tilde{\tilde{\tau}}_{r,c} - \Delta\delta\tilde{\tilde{\tau}}^{k,c}) - \lambda_m \tilde{\beta}_m^{k,c} + \varepsilon_{r,m}^k & r = \mathrm{ref}, k \neq \mathrm{ref} \\ c\delta\tilde{\tilde{\tau}}_{r,c} - \lambda_m \tilde{\beta}_m^{k,c} + \varepsilon_{r,m}^k & r = \mathrm{ref}, k = \mathrm{ref}. \end{cases}\end{aligned} \qquad (19)$$

$$\begin{aligned}\tilde{\rho}_{r,m}^k &= (\mathbf{e}_r^k)^{\mathrm{T}}(-\Delta \mathbf{x}^k) + m_{\mathrm{T}}(E_r^k) T_{\mathrm{z},r} + q_{1m}^2 \tilde{I}_{r,1}^k \\ &+ \begin{cases} c(\delta\tilde{\tilde{\tau}}_{r,c} - \Delta\delta\tilde{\tilde{\tau}}^{k,c}) + \Delta\rho_{\mathrm{MP}_{r,m}}^k + \eta_{r,m}^k & r \neq \mathrm{ref}, k \neq \mathrm{ref} \\ c\delta\tilde{\tilde{\tau}}_{r,c} + \Delta\rho_{\mathrm{MP}_{r,m}}^k + \eta_{r,m}^k & r \neq \mathrm{ref}, k = \mathrm{ref} \\ c(\delta\tilde{\tilde{\tau}}_{r,c} - \Delta\delta\tilde{\tilde{\tau}}^{k,c}) + \Delta\rho_{\mathrm{MP}_{r,m}}^k + \eta_{r,m}^k & r = \mathrm{ref}, k \neq \mathrm{ref} \\ c\delta\tilde{\tilde{\tau}}_{r,c} + \Delta\rho_{\mathrm{MP}_{r,m}}^k + \eta_{r,m}^k & r = \mathrm{ref}, k = \mathrm{ref}. \end{cases}\end{aligned} \qquad (20)$$

5 Cluster solution with Kalman filter

In this section, we briefly describe the estimation of satellite positions, clock offsets and phase biases for an individual cluster.

The corrected carrier phase and pseudorange measurements of all receivers $r \in \{1, \ldots, R\}$ and frequencies $m \in \{1, \ldots, M\}$ in cluster c of a certain epoch are stacked in a column vector, i.e.

$$
\begin{aligned}
z^c = \Big(& \lambda_1 \tilde{\varphi}_{1,1}^1, \ldots, \lambda_1 \tilde{\varphi}_{1,1}^K, \ldots, \lambda_1 \tilde{\varphi}_{R,1}^1, \ldots, \lambda_1 \tilde{\varphi}_{R,1}^K, \ldots \\
& \lambda_M \tilde{\varphi}_{1,M}^1, \ldots, \lambda_M \tilde{\varphi}_{1,M}^K, \ldots, \lambda_M \tilde{\varphi}_{R,M}^1, \ldots, \lambda_M \tilde{\varphi}_{R,M}^K, \\
& \tilde{\rho}_{1,1}^1, \ldots, \tilde{\rho}_{1,1}^K, \ldots, \tilde{\rho}_{R,1}^1, \ldots, \tilde{\rho}_{R,1}^K, \ldots, \\
& \tilde{\rho}_{1,M}^1, \ldots, \tilde{\rho}_{1,M}^K, \ldots, \tilde{\rho}_{R,M}^1, \ldots, \tilde{\rho}_{R,M}^K \Big)^{\mathrm{T}}.
\end{aligned} \tag{21}
$$

Similarly, all unknowns of cluster c are stacked in the state vector x^c given by

$$
x^c = \begin{pmatrix} x_{\mathrm{real}}^c \\ x_{\mathrm{int}}^c \end{pmatrix} \tag{22}
$$

with the real-valued state parameters

$$
\begin{aligned}
x_{\mathrm{real}}^c = \Big(& (\Delta \mathbf{x}^1)^{\mathrm{T}}, \ldots, (\Delta \mathbf{x}^K)^{\mathrm{T}}, \\
& c\delta\tilde{\tilde{\tau}}_{1,c}, \ldots, c\delta\tilde{\tilde{\tau}}_{R,c}, c\Delta\delta\tilde{\tilde{\tau}}^{1,c}, \ldots, c\Delta\delta\tilde{\tilde{\tau}}^{K,c}, \\
& T_{z,1}, \ldots, T_{z,R}, \\
& \tilde{I}_{1,1}^1, \ldots, \tilde{I}_{1,1}^K, \ldots, \tilde{I}_{R,1}^1, \ldots, \tilde{I}_{R,1}^K, \\
& \tilde{\beta}_{1,c,1}, \ldots, \tilde{\beta}_{R,c,1}, \ldots, \tilde{\beta}_{1,c,M}, \ldots, \tilde{\beta}_{R,c,M}, \\
& \tilde{\beta}_1^{1,c}, \ldots, \tilde{\beta}_1^{K,c}, \ldots, \tilde{\beta}_M^{1,c}, \ldots, \tilde{\beta}_M^{K,c} \Big)^{\mathrm{T}},
\end{aligned} \tag{23}
$$

and the integer-valued state parameters

$$
\begin{aligned}
x_{\mathrm{int}}^c = \Big(& \tilde{N}_{1,c,1}^1, \ldots, \tilde{N}_{1,c,1}^K, \ldots, \tilde{N}_{R,c,1}^1, \ldots, \tilde{N}_{R,c,1}^K, \ldots, \\
& \tilde{N}_{1,c,M}^1, \ldots, \tilde{N}_{1,c,M}^K, \ldots, \tilde{N}_{R,c,M}^1, \ldots, \tilde{N}_{R,c,M}^K \Big)^{\mathrm{T}}.
\end{aligned} \tag{24}
$$

The conditioning of the system of observation equations can be substantially improved by using prior information on the state parameters. The satellite positions and clock offsets are known, e.g. from the broadcast orbits with an accuracy of 1 m and 1.5 m. Blind tropospheric models (i.e. without using current meteorological observations) provide the hydrostatic part of the tropospheric delay with centimetre-level accuracy. The fractional part of the satellite phase biases is in the order of a few centimetres. The ionospheric delay could be obtained from any local augmentation service with centimetre accuracy or from the Klobuchar model with meter-level accuracy. Therefore, we introduce some *prior* knowledge on these state parameters:

$$
\begin{aligned}
\bar{x}^c = \Big(& (\Delta \bar{\mathbf{x}}^1)^{\mathrm{T}}, \ldots, (\Delta \bar{\mathbf{x}}^K)^{\mathrm{T}}, \\
& c\Delta\delta\bar{\tilde{\tau}}^{1,c}, \ldots, c\Delta\delta\bar{\tilde{\tau}}^{K,c}, \\
& \bar{T}_{z,1}, \ldots, \bar{T}_{z,R}, \bar{\tilde{I}}_{1,1}^1, \ldots, \bar{\tilde{I}}_{1,1}^K, \ldots, \bar{\tilde{I}}_{R,1}^1, \ldots, \bar{\tilde{I}}_{R,1}^K, \\
& \bar{\tilde{\beta}}_{1,c,1}, \ldots, \bar{\tilde{\beta}}_{R,c,1}, \ldots, \bar{\tilde{\beta}}_{1,c,M}, \ldots, \bar{\tilde{\beta}}_{R,c,M}, \\
& \bar{\tilde{\beta}}_1^{1,c}, \ldots, \bar{\tilde{\beta}}_1^{K,c}, \ldots, \bar{\tilde{\beta}}_M^{1,c}, \ldots, \bar{\tilde{\beta}}_M^{K,c} \Big)^{\mathrm{T}},
\end{aligned} \tag{25}
$$

with a priori known covariance matrix $\Sigma_{\bar{x}^c}$. As the orbital errors are small compared to the receiver–satellite ranges, it can be assumed that both measurements and prior information are linear functions of the state vector of Eq. (23). Thus, z^c and $\bar{x}^c$ are combined to

$$
\begin{pmatrix} z^c \\ \bar{x}^c \end{pmatrix} = \left(H_{\mathrm{real}}^c, H_{\mathrm{int}}^c \right) \begin{pmatrix} x_{\mathrm{real}}^c \\ x_{\mathrm{int}}^c \end{pmatrix} + \begin{pmatrix} \eta_z^c \\ \eta_{\bar{x}}^c \end{pmatrix}, \tag{26}
$$

where the state-to-measurement mapping matrices H_{real}^c and H_{int}^c are implicitly defined by Eqs. (19) and (20) and η_z^c and $\eta_{\bar{x}}^c$ denote the measurement noise and error of the prior information. We assume that both errors can be modelled by white Gaussian noise and refer to Bryson and Henrikson (1968) for precise modelling of coloured noise.

We use a standard Kalman filter [see Brown and Hwang (2012)] to estimate x^c from the extended measurement vector and denote the resulting state estimate by $(\hat{x}^c)^+$. The estimated state vector also includes $M \cdot \sum_{r=1, r\neq \mathrm{ref}}^{R} (K_r - 1)$ double- difference ambiguities. A typical cluster with $R = 40$ dual-frequency receivers and an average of 9 visible satellites per receiver results in $2 \cdot (40-1) \cdot (9-1) = 624$ double difference ambiguities. The large number of a few hundreds of ambiguities puts some computational constraints on the fixing. Unfortunately, a tree search as used in the Least-squares AMBiguity Decorrelation Adjustment (LAMBDA) method of Teunissen (1995) is no longer feasible. However, a sequential fixing with integer decorrelation is still feasible. The fixed ambiguities are obtained as

$$
\check{\tilde{N}}_c = Z_c^{-1} \mathcal{F}_c \left(Z_c \hat{\tilde{N}}_c \right), \tag{27}
$$

with the integer decorrelation transformation Z_c, the fixing $\mathcal{F}_c$ and the float ambiguity estimates $\hat{\tilde{N}}_c$. The latter one includes the float double- difference ambiguities of all receivers, frequencies and satellites of cluster c, i.e.

$$
\begin{aligned}
\hat{\tilde{N}}_c = \Big(& \hat{\tilde{N}}_{1,c,1}^1, \ldots, \hat{\tilde{N}}_{1,c,1}^K, \ldots, \hat{\tilde{N}}_{R,c,1}^1, \\
& \ldots, \hat{\tilde{N}}_{R,c,1}^K, \ldots, \hat{\tilde{N}}_{R,c,M}^K \Big)^{\mathrm{T}}.
\end{aligned} \tag{28}
$$

The integer decorrelation Z_c is given by Teunissen (1995) as an alternating sequence of a pairwise integer decorrelation Z_c^i and permutation P_c^i, i.e.

$$Z_c = \prod_{i=1}^{n_{\text{iter}}} Z_c^i P_c^i. \tag{29}$$

The number of iterations n_{iter} grows exponentially with the number of ambiguities. However, a partial integer decorrelation with a limited number of iterations is still always feasible. Henkel and Günther (2010) have shown that a partial integer decorrelation enables an attractive trade-off between variance reduction and bias amplification for bootstrapping. The fixing $\mathcal{F}_c$ includes a sequential rounding of the conditional float ambiguities to the nearest integer number:

$$\check{\tilde{N}}_{r,c,m}^{k} = \mathcal{F}_c\left(\hat{\tilde{N}}_{r,c,m}^{k|1,\ldots,k-1}\right) = \left[\hat{\tilde{N}}_{r,c,m}^{k|1,\ldots,k-1}\right], \tag{30}$$

where the kth conditional float ambiguity estimate is given by Blewitt (1989) as

$$\hat{\tilde{N}}_{r,c,m}^{k|1,\ldots,k-1} = \hat{\tilde{N}}_{r,c,m}^{k} - \sum_{j=1}^{k-1} \gamma_{r,c,m}^{kj} (\hat{\tilde{N}}_{r,c,m}^{j|1,\ldots,j-1} - [\hat{\tilde{N}}_{r,c,m}^{j|1,\ldots,j-1}]), \tag{31}$$

with the coefficient

$$\gamma_{r,c,m}^{kj} = \sigma_{\hat{\tilde{N}}_{r,c,m}^{k} \hat{\tilde{N}}_{r,c,m}^{j|1,\ldots,j-1}} / \sigma^2_{\hat{\tilde{N}}_{r,c,m}^{j|1,\ldots,j-1}}. \tag{32}$$

The latter one only depends on the float ambiguity covariance matrix, that is, part of the state covariance matrix of the Kalman filter. Once the ambiguities are fixed, the real-valued state estimates of Eq. (23) are readjusted by linear least-squares estimation, i.e.

$$\begin{aligned}\check{x}_{\text{real}}^c &= \arg\min_{x_{\text{real}}^c} \left\| z^c - H_{\text{int}}^c \check{x}_{\text{int}}^c - H_{\text{real}}^c x_{\text{real}}^c \right\|^2_{\Sigma_{z^c}^{-1}} \\ &= \left((H_{\text{real}}^c)^{\mathrm{T}} \Sigma_{z^c}^{-1} H_{\text{real}}^c \right)^{-1} (H_{\text{real}}^c)^{\mathrm{T}} \Sigma_{z^c}^{-1} \left(z^c - H_{\text{int}}^c \check{x}_{\text{int}}^c \right),\end{aligned} \tag{33}$$

where Σ_{z^c} denotes the measurement covariance matrix for cluster c.

6 Combination of clusters

This section describes the combination of the satellite positions, clock offsets and phase bias estimates of all clusters. We derive a multi-cluster solution to achieve the following benefits:

- satellites being *visible from more than one cluster* provide *multiple correlated* satellite position, clock and phase bias estimates
- selection of a reference cluster c_{ref} enables expression of satellite phase biases of any cluster in terms of satellite phase biases of reference cluster
- satellite phase bias estimates of any cluster differ from the satellite phase bias estimates of the reference cluster only by a cluster-dependent bias being common to all satellites and by differential *integer* ambiguities

The satellite position correction estimate of cluster c is provided by the Kalman filter and modelled as

$$\left(\Delta\hat{\mathbf{x}}^{k,c}\right)^+ = \Delta\mathbf{x}^k + \eta_{\Delta\hat{\mathbf{x}}^{k,c}}, \tag{34}$$

with the true cluster-independent position correction $\Delta\mathbf{x}^k$ and the estimation error $\eta_{\Delta\hat{\mathbf{x}}^{k,c}}$. Estimates are denoted by $\hat{}$, and state updates are additionally indicated by $(\cdot)^+$.

The estimates of the cluster-dependent satellite clock offsets of Eq. (14) are related to the satellite clock offsets of the reference cluster and differential (cluster to reference cluster) satellite clock offsets, i.e.

$$\begin{aligned}\left(c\Delta\delta\hat{\tilde{\tilde{\tau}}}^{k,c}\right)^+ &:= c\left(\Delta\delta\tau^k - \Delta\delta\tau^{\text{ref}(c)}\right) \\ &\quad + \sum_{m=1}^{M} \gamma_{1m} \cdot (b_m^k - b_m^{\text{ref}(c)}) + \eta_{c\Delta\delta\hat{\tilde{\tilde{\tau}}}^{k,c}} \\ &= \left(c\Delta\delta\hat{\tilde{\tilde{\tau}}}^{k,c_{\text{ref}}}\right)^+ - \left(c\Delta\delta\hat{\tilde{\tilde{\tau}}}^{\text{ref}(c),c_{\text{ref}}}\right)^+\end{aligned} \tag{35}$$

The estimates of the satellite phase biases $\tilde{\beta}_m^{k,c}$ of Eq. (17) include satellite and/ or cluster-dependent parameters. Therefore, we rewrite the satellite phase bias estimates as

$$\left(\lambda_m\hat{\tilde{\beta}}_m^{k,c}\right)^+ = u_m^k + v_{c,m} + w_{c,m}^k + \eta_{\lambda_m\tilde{\beta}_m^{k,c}}, \tag{36}$$

with

$$\begin{aligned}u_m^k &= \lambda_m\beta_m^k - \sum_{m=1}^{M}(\gamma_{1m} - q_{1m}^2\gamma_{2m})b_m^k \\ v_{c,m} &= -\lambda_m\beta_{\text{ref}(c),m} + \sum_{m=1}^{M}(\gamma_{1m} - q_{1m}^2\gamma_{2m})b_{\text{ref}(c),m} \\ w_{c,m}^k &= -\lambda_m N_{\text{ref}(c),m}^k.\end{aligned} \tag{37}$$

The satellite phase bias estimates of any cluster c can be related to the satellite phase bias estimates of the reference cluster, i.e.

$$\begin{aligned}\left(\lambda_m\hat{\tilde{\beta}}_m^{k,c}\right)^+ &= u_m^k + v_{c_{\text{ref}},m} + w_{c_{\text{ref}},m}^k \\ &\quad + (v_{c,m} - v_{c_{\text{ref}},m}) \\ &\quad + (w_{c,m}^k - w_{c_{\text{ref}},m}^k) + \eta_{\lambda_m\tilde{\beta}_m^{k,c}}.\end{aligned} \tag{38}$$

The first three terms can be combined to

$$\tilde{u}_m^k := u_m^k + v_{c_{\mathrm{ref}},m} + w_{c_{\mathrm{ref}},m}^k, \tag{39}$$

which is of dimension KM. As a separate determination of $\tilde{u}_m^k$, $v_{c,m}$ and $w_{c,m}^k$ from $(\lambda_m \hat{\tilde{\beta}}_m^{k,c})^+$ is not feasible due to rank deficiency and as the integer property of $w_{c,m}^k$ shall be exploited, we select a satellite k that is visible both at cluster c and cluster c_{ref} as dual-cluster reference satellite (being denoted by $\overline{\mathrm{ref}}(c)$) and map the differential ambiguity $w_{c,m}^{\overline{\mathrm{ref}}(c)} - w_{c_{\mathrm{ref}},m}^{\overline{\mathrm{ref}}(c)}$ to $v_{c,m}$. Thus, the satellite phase bias estimate is expressed in terms of the reduced parameter set:

$$\left(\lambda_m \hat{\tilde{\beta}}_m^{k,c}\right)^+ = \tilde{u}_m^k + \tilde{v}_{c,m} + \tilde{w}_{c,m}^k + \eta_{\lambda_m \tilde{\beta}_m^{k,c}}, \tag{40}$$

with

$$\tilde{v}_{c,m} = v_{c,m} - v_{c_{\mathrm{ref}},m} + \left(w_{c,m}^{\overline{\mathrm{ref}}(c)} - w_{c_{\mathrm{ref}},m}^{\overline{\mathrm{ref}}(c)}\right) \quad \forall\, c \neq c_{\mathrm{ref}}, m \tag{41}$$

$$\tilde{w}_{c,m}^k = \left(w_{c,m}^k - w_{c_{\mathrm{ref}},m}^k\right) - \left(w_{c,m}^{\overline{\mathrm{ref}}(c)} - w_{c_{\mathrm{ref}},m}^{\overline{\mathrm{ref}}(c)}\right) \quad \forall\, k \neq \overline{\mathrm{ref}}(c), c \neq c_{\mathrm{ref}}, m \tag{42}$$

The phase bias decomposition of Eq. (40) into a common satellite phase bias $\tilde{u}_m^k$, a cluster-dependent offset $\tilde{v}_{c,m}$ and integer ambiguities $\tilde{w}_{c,m}^k$ is the basis for the combination of bias estimates from individual clusters. Seepersad et al. (2016) combined the clock products from various analysis centres with a very similar approach to enable precise positioning with integer ambiguity resolution at the end user. The meaning, dimensions and notation of the reduced parameter set are summarized in Table 1.

We derive the multi-cluster solution of satellite positions, clock offsets and phase biases from the single-cluster solutions of the Kalman filter. As the Kalman filter considers the measurements of all previous epochs, it is sufficient to stack the a posteriori state estimates of all clusters of the current epoch in a column vector:

$$\begin{aligned} z = \Big(& ((\Delta\hat{\mathbf{x}}^{1,1})^+)^{\mathrm{T}}, \ldots, ((\Delta\hat{\mathbf{x}}^{K,1})^+)^{\mathrm{T}}, \ldots, ((\Delta\hat{\mathbf{x}}^{1,C})^+)^{\mathrm{T}}, \ldots, \\ & ((\Delta\hat{\mathbf{x}}^{K,C})^+)^{\mathrm{T}}, (\Delta\delta\hat{\tilde{\tau}}^{1,1})^+, \ldots, (\Delta\delta\hat{\tilde{\tau}}^{K,1})^+, \ldots, \\ & (\Delta\delta\hat{\tilde{\tau}}^{1,C})^+, \ldots, (\Delta\delta\hat{\tilde{\tau}}^{K,C})^+, (\lambda_m\hat{\tilde{\beta}}_1^{1,1})^+, \ldots, \\ & (\lambda_m\hat{\tilde{\beta}}_1^{K,1})^+, \ldots, (\lambda_m\hat{\tilde{\beta}}_M^{1,1})^+, \ldots, (\lambda_m\hat{\tilde{\beta}}_M^{K,1})^+, \ldots \\ & (\lambda_m\hat{\tilde{\beta}}_1^{1,C})^+, \ldots, (\lambda_m\hat{\tilde{\beta}}_1^{K,C})^+, \ldots, \\ & (\lambda_m\hat{\tilde{\beta}}_M^{1,C})^+, \ldots, (\lambda_m\hat{\tilde{\beta}}_M^{K,C})^+\Big)^{\mathrm{T}}, \end{aligned} \tag{43}$$

where we assumed that the clusters are not overlapping, i.e. there are no shared receivers among clusters. The stacked estimates of all clusters are considered as *measurements* that are linearly related to the satellite positions, clock offsets and phase biases, i.e.

$$z = Hx + \eta_z, \tag{44}$$

where the mapping matrix H and the state vector x can be split into a part referring to *real*-valued states and a part referring to *integer*-valued states:

$$H = (H_{\mathrm{real}}, H_{\mathrm{int}}), \tag{45}$$

and

$$x = \begin{pmatrix} x_{\mathrm{real}} \\ x_{\mathrm{int}} \end{pmatrix}, \tag{46}$$

where x_{real} and x_{int} are defined as

$$\begin{aligned} x_{\mathrm{real}} = \Big(& (\Delta\mathbf{x}^1)^{\mathrm{T}}, \ldots, (\Delta\mathbf{x}^K)^{\mathrm{T}}, \\ & c\Delta\delta\tilde{\tilde{\tau}}^{1,c_{\mathrm{ref}}}, \ldots, c\Delta\delta\tilde{\tilde{\tau}}^{K,c_{\mathrm{ref}}}, \\ & c\Delta\delta\tilde{\tilde{\tau}}^{\mathrm{ref}(1),c_{\mathrm{ref}}}, \ldots, c\Delta\delta\tilde{\tilde{\tau}}^{\mathrm{ref}(C),c_{\mathrm{ref}}}, \\ & \tilde{u}_1^1, \ldots, \tilde{u}_1^K, \ldots, \tilde{u}_M^1, \ldots, \tilde{u}_M^K, \\ & \tilde{v}_{1,1}, \ldots, \tilde{v}_{C,1}, \ldots, \tilde{v}_{1,M}, \ldots, \tilde{v}_{C,M}\Big)^{\mathrm{T}}, \end{aligned} \tag{47}$$

and

$$\begin{aligned} x_{\mathrm{int}} = \Big(& \tilde{w}_{1,1}^1, \ldots, \tilde{w}_{1,1}^K, \ \ldots \tilde{w}_{C,1}^1, \ldots, \tilde{w}_{C,1}^K, \ldots \\ & \tilde{w}_{1,M}^1, \ldots, \tilde{w}_{1,M}^K, \ \ldots \ \tilde{w}_{C,M}^1, \ldots, \tilde{w}_{C,M}^K\Big)^{\mathrm{T}}, \end{aligned} \tag{48}$$

and η_z denotes the measurement noise. We obtain the measurement covariance matrix from the covariance matrix of the posteriori state estimate of the Kalman filter, i.e. $\Sigma_z = \Sigma_{\hat{x}^+}$. The weighted least-squares solution of x is given by

$$\hat{x} = \arg\min_x \|z - Hx\|^2_{\Sigma_z^{-1}} = (H^{\mathrm{T}}\Sigma_z^{-1}H)^{-1}H^{\mathrm{T}}\Sigma_z^{-1}z. \tag{49}$$

The number of ambiguities in $\hat{x}$ is for typical values of K, C and M much larger than the number of satellite positions, clock offsets and phase biases. Therefore, the ambiguity fixing of the multi-cluster combination is very beneficial. The ambiguity fixing is performed again with bootstrapping and integer decorrelation as described in Eqs. (27)–(32). The real-valued states x_{real} are readjusted after ambiguity fixing as

$$\check{x}_{\mathrm{real}} = \left(H_{\mathrm{real}}^{\mathrm{T}}\Sigma_z^{-1}H_{\mathrm{real}}\right)^{-1} H_{\mathrm{real}}^{\mathrm{T}}\Sigma_z^{-1}\left(z - H_{\mathrm{int}}\check{x}_{\mathrm{int}}\right). \tag{50}$$

The obtained satellite position, clock offset and phase bias corrections enable precise point positioning with integer ambiguity resolution as described in the next section.

Table 1 Main characteristics of the reduced parameter set for the combined solution of multiple clusterwise solutions

	Notation	Dimensions	Lumped parameters
Satellite phase biases	$\tilde{u}_m^k$	KM	Satellite code biases
			Receiver phase and code biases of ref. receiver at ref. cluster
			Integer ambiguity of ref. receiver at ref. cluster
Receiver phase biases	$\tilde{v}_{c,m}$	$(C-1)M$	Receiver phase bias of ref. receiver at ref. cluster
			Integer ambiguities of ref. receiver at cluster and ref.cluster
Double difference integer ambiguities between ref. receivers at ref. cluster and any other cluster	$\tilde{w}_{c,m}^k$	$(C-1)M(K-1)$	

C, K and M denote the number of clusters, satellites and frequencies

7 Precise point positioning with satellite position, clock and phase bias corrections

In this section, the application of the satellite position, clock and phase bias corrections for precise point positioning of any user is described. The user's parameter mapping is assumed to be equal to the parameter mapping of the reference network.

The user u corrects its phase measurements for the known Earth tides, satellite position estimate $\hat{x}_u^k$, satellite position *correction* estimate $\Delta\hat{x}^k$, satellite clock offset estimate $\delta\hat{\tau}^k$, satellite clock offset *correction* estimates $\Delta\delta\hat{\hat{\tilde{\tau}}}^{k,c_{\text{ref}}}$ and $\Delta\delta\hat{\hat{\tilde{\tau}}}^{\text{ref}(c),c_{\text{ref}}}$, and satellite phase bias estimate $\hat{\tilde{u}}_m^k$, i.e.

$$\lambda_m\tilde{\varphi}_{u,c,m}^k := \lambda_m\varphi_{u,m}^k - (\mathbf{e}_u^k)^{\text{T}}\left(\Delta\mathbf{x}_{\text{ET},u} - (\hat{\mathbf{x}}_u^k + \Delta\hat{\mathbf{x}}^k)\right) + c\left(\delta\hat{\tau}^k + \Delta\delta\hat{\hat{\tilde{\tau}}}^{k,c_{\text{ref}}} - \Delta\delta\hat{\hat{\tilde{\tau}}}^{\text{ref}(c),c_{\text{ref}}}\right) - \hat{\tilde{u}}_m^k - \lambda_m\left(\Delta\varphi_{\text{PW},u}^k + \Delta\varphi_{\text{PCO},u,m}^k + \Delta\varphi_{\text{PCV},u,m}^k\right) \tag{51}$$

We replace the phase measurement $\lambda_m\varphi_{u,m}^k$ by its model, use Eq. (39) and assume that the residual orbital and clock errors are negligible to obtain

$$\lambda_m\tilde{\varphi}_{u,m}^k \approx (\mathbf{e}_u^k)^{\text{T}}\mathbf{x}_u + c\delta\tau_u + \lambda_m N_{u,m}^k - \hat{w}_{c_{\text{ref}},m}^k + \lambda_m\beta_{u,m} - \hat{v}_{c_{\text{ref}},m} + m_{\text{T}}(E_u^k)T_{z,u} - q_{1m}^2\tilde{I}_{u,1}^k + \varepsilon_{u,m}^k. \tag{52}$$

The ambiguity $\hat{w}_{c_{\text{ref}},m}^k$ of the reference receiver of the reference cluster is mapped to the user ambiguity, i.e.

$$\tilde{N}_{u,m}^k := N_{u,m}^k - \hat{w}_{c_{\text{ref}},m}^k/\lambda_m \overset{!}{\in} \mathbb{Z}, \tag{53}$$

i.e. the precise point positioning user only needs to estimate this differential ambiguity. Similarly, the phase bias $\hat{v}_{c_{\text{ref}},m}$ of the reference receiver of the reference cluster is mapped to the receiver phase bias, i.e.

$$\tilde{\beta}_{u,m} := \beta_{u,m} - \hat{v}_{c_{\text{ref}},m}. \tag{54}$$

Thus, the user's measurement model of Eq. (52) can be rewritten as

$$\lambda_m\tilde{\varphi}_{u,m}^k \approx (\mathbf{e}_u^k)^{\text{T}}\mathbf{x}_u + c\delta\tau_u + \lambda_m\tilde{N}_{u,m}^k + \lambda_m\tilde{\beta}_{u,m} + m_{\text{T}}(E_u^k)T_{z,u} - q_{1m}^2\tilde{I}_{u,1}^k + \varepsilon_{u,m}^k. \tag{55}$$

The receiver clock offset and phase biases can be eliminated by considering the difference between two satellites k and l:

$$\lambda_m\tilde{\varphi}_{u,m}^{kl} \approx (\mathbf{e}_u^{kl})^{\text{T}}\mathbf{x}_u + \lambda_m\tilde{N}_{u,m}^{kl} + (m_{\text{T}}(E_u^k) - m_{\text{T}}(E_u^l))T_{z,u} - q_{1m}^2\tilde{I}_{u,1}^{kl} + \varepsilon_{u,m}^{kl}, \tag{56}$$

which corresponds to the measurement model of Kouba and Héroux (2001) for precise point positioning with integer ambiguity resolution.

8 Simulation results

In this section, the performance of the proposed dual stage multi-cluster based estimation of satellite position, clock and phase bias corrections, tropospheric zenith and ionospheric slant delays and integer ambiguities is analysed. Galileo measurements on the frequencies E1 and E5a of the full Galileo constellation (27 satellites) are simulated for the 424 stations of the global IGS network. The IGS stations are grouped into 16 clusters as shown in Fig. 2. The measurement noise was simulated as white Gaussian noise. In particular, a standard deviation of 2 mm is assumed for the phase noise and of 20 cm for the pseudorange noise. Thousand epochs are simulated with a sampling interval of 100 s resulting in a total time period of 1 day, 3 hours and 2800 s.

The process noise of the receiver and satellite clock offsets is modelled by a standard deviation of 1 m/epoch. The satellite position corrections, receiver and satellite phase biases, tropospheric zenith delays and ionospheric slant delays are modelled by a random-walk process with a standard deviation of 1 mm/epoch.

The objective of this work is the estimation of corrections for the broadcast satellite positions and clock offsets and of additional satellite phase biases without using any precise orbits and clocks. Therefore, we assume to know only the accuracy of the broadcast satellite positions and clock offset *corrections* but not their actual errors, i.e. the prior information is modelled as

$$\Delta\bar{\mathbf{x}}^k_{x,y,z} = 0\,\mathrm{m}, \quad \sigma_{\Delta\bar{\mathbf{x}}^k_{x,y,z}} = 1.0\,\mathrm{m} \quad \forall\, k, c$$
$$c\Delta\delta\tilde{\bar{\tau}}^{k,c} = 0\,\mathrm{m}, \quad \sigma_{c\Delta\delta\tilde{\bar{\tau}}^{k,c}} = 1.5\,\mathrm{m} \quad \forall\, k, c. \tag{57}$$

8.1 Benefit of integer decorrelation

In this subsection, the benefit of integer decorrelation is analysed for high-dimensional ambiguity fixing within one of the largest clusters. The success rate for sequential ambiguity fixing/ bootstrapping is given by Teunissen (1998) as

$$P_{\mathrm{s}}^c = \prod_{r=1}^{R_c}\prod_{m=1}^{M}\int_{-0.5}^{+0.5}\frac{1}{\sqrt{2\pi\sigma^2_{\hat{\tilde{N}}^{j|1,\ldots,j-1}_{r,c,m}}}}\, e^{-\frac{\varepsilon^2}{2\sigma^2_{\hat{\tilde{N}}^{j|1,\ldots,j-1}_{r,c,m}}}}\, d\varepsilon, \tag{58}$$

where the variances $\sigma^2_{\hat{\tilde{N}}^{j|1,\ldots,j-1}_{r,c,m}}$ of the conditional ambiguity estimates are obtained from the triangular decomposition of the float ambiguity covariance matrix. The variances of the conditional ambiguities depend on the integer decorrelation and permutation transformation $\boldsymbol{Z}^c$ of Eq. (29) due to its permutations.

Figure 3 shows the success rate of ambiguity fixing for the Western American cluster with 54 receivers over time. Obviously, the success rate increases with time due to the convergence of the Kalman filter. The speed of convergence depends significantly on the number n_{iter} of pairwise decorrelations and permutations. A success rate of 90% is achieved only after 100 s if no integer decorrelation is used. Today's orbit and clock determination software packages, e.g. the bernese GNSS software as described by Dach et al. (2007), do not use an integer decorrelation and permutation transformation. However, a substantial reduction in the convergence time is achieved by using this transformation. The tremendous benefit arises from the exploitation of the strong correlations between the 1227 ambiguities. It shall be noted that the full benefit can be achieved only if the statistics of the

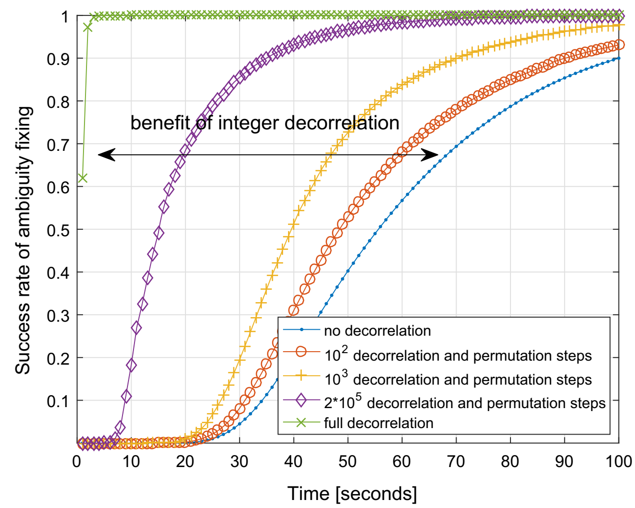

Fig. 3 Success rate of high-dimensional sequential integer ambiguity fixing of the Western American cluster with 54 receivers: a success rate of 90% is achieved only after 100 s if no integer decorrelation is used. The integer decorrelation enables a drastic reduction in the fixing time to a few seconds

float solution are accurately known. If the statistics are significantly biased, it is preferable to use only a partial integer decorrelation with a limited number of iterations n_{iter}.

8.2 Benefit of ambiguity fixing and of multiple clusters

In this section, the benefit of ambiguity fixing and of multiple clusters is analysed. The convergence of the satellite position corrections of the multi-cluster combination is shown for float ambiguities in Fig. 4 and for fixed ambiguities in Fig. 5. The float solution requires approximately 150 epochs (4 hours) to converge to a level with errors of less than 5 cm. The errors remain for almost all satellites and epochs below this threshold except for a few epochs, where some satellites show a larger error due to weak observability. However, a much faster convergence and higher stability over time can be observed after fixing of the real-valued ambiguity estimates to their integer values.

In particular, it can be observed that the accuracy is better than 3 cm for almost all epochs and satellites after the initial convergence. The errors reduce to less than 5 cm within 20 epochs (33 min) and to less than 3 cm within 40 epochs (66 min). Figure 6 shows the accuracy of the satellite phase bias estimates referring to the reference cluster. The errors are below 0.2 cycles (4 cm) for all satellites and epochs except of a few epochs, where some satellites are only weakly observable at the reference cluster. The fixed solution is provided in Fig. 7 and shows a lower noise level and higher stability than the float solution. One can also observe a high correlation

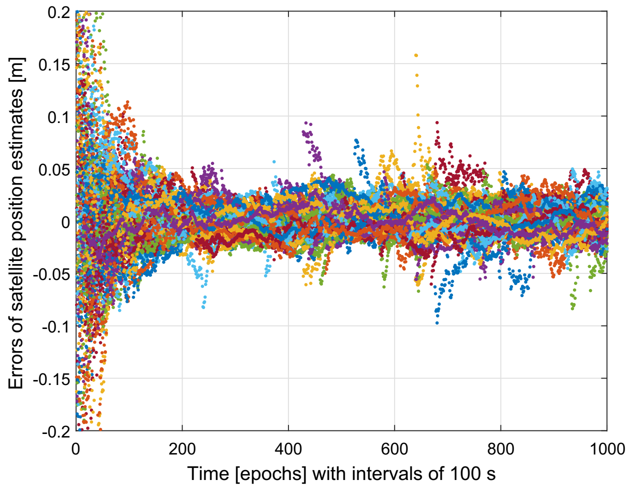

Fig. 4 Errors of multi-cluster satellite position correction estimates with **float** ambiguities. Each colour represents a different satellite

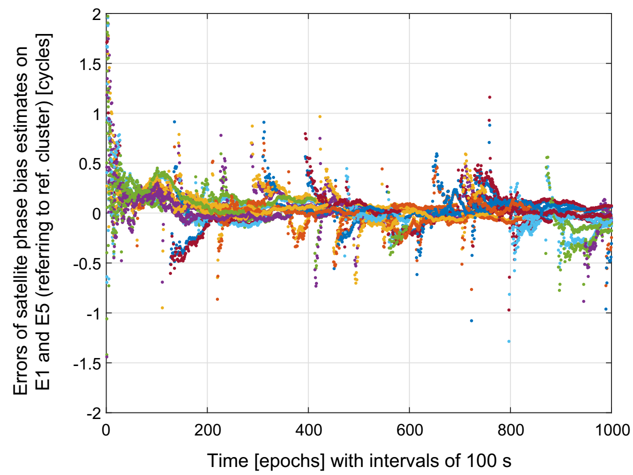

Fig. 6 Errors of multi-cluster satellite phase bias estimates on E1 and E5a (referring to the reference cluster) with **float** ambiguities. Each colour represents a different satellite

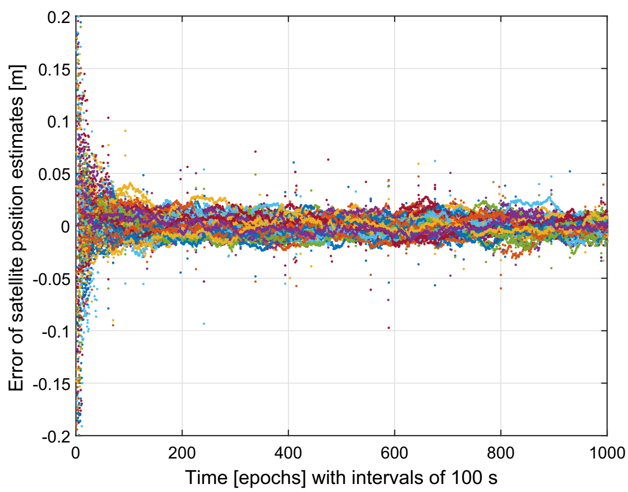

Fig. 5 Errors of multi-cluster satellite position correction estimates with **fixed** ambiguities. Each colour represents a different satellite

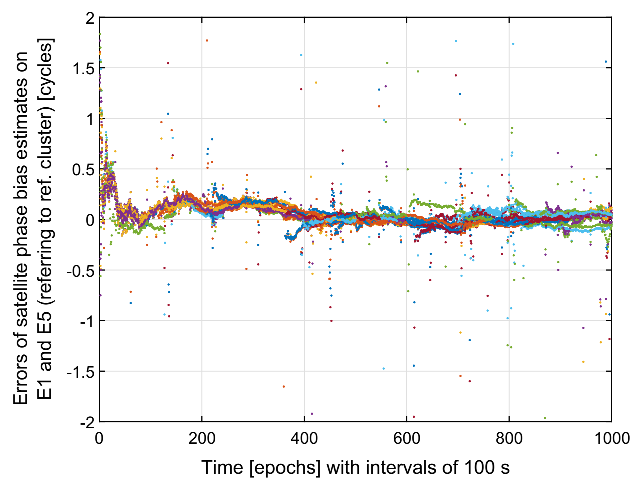

Fig. 7 Errors of multi-cluster satellite phase bias estimates on E1 and E5a (referring to the reference cluster) with **fixed** ambiguities. Each colour represents a different satellite

between the errors of the satellite phase bias estimates from different satellites.

Figure 8 shows the benefit in precision of the *multi*-cluster over the *single*-cluster solution of satellite position corrections, satellite clock offsets and satellite phase biases. The ambiguities were estimated as float values. The subfigures on the left side refer to the single cluster, and those on the right side refer to the multi-cluster solution. Each plotted line refers to a satellite pass.

It can be clearly seen that the single-cluster solution has a poor precision for the parameters related to satellites rising at the edge of the cluster. On the contrary, the multi-cluster solution provides satellite position corrections, satellite clock offsets and phase biases with a precision varying between 8 and 50 mm for all satellites and epochs after initial convergence. In addition, a faster convergence and a lower error floor can be observed especially for the satellite position and clock errors of the multi-cluster combined solution.

The ambiguity-fixed solution is shown for the same scenario and parameters in Fig. 9. The convergence time is significantly shorter for both the single- and multi-cluster solutions. A higher precision is also achieved for the multi-cluster solution of satellite position corrections, satellite clock offsets and phase biases with a standard deviation between 5 and 20 mm for all satellites.

9 Real data analysis

In this section, we validate the proposed estimation of satellite position, clock and phase bias corrections, tropospheric

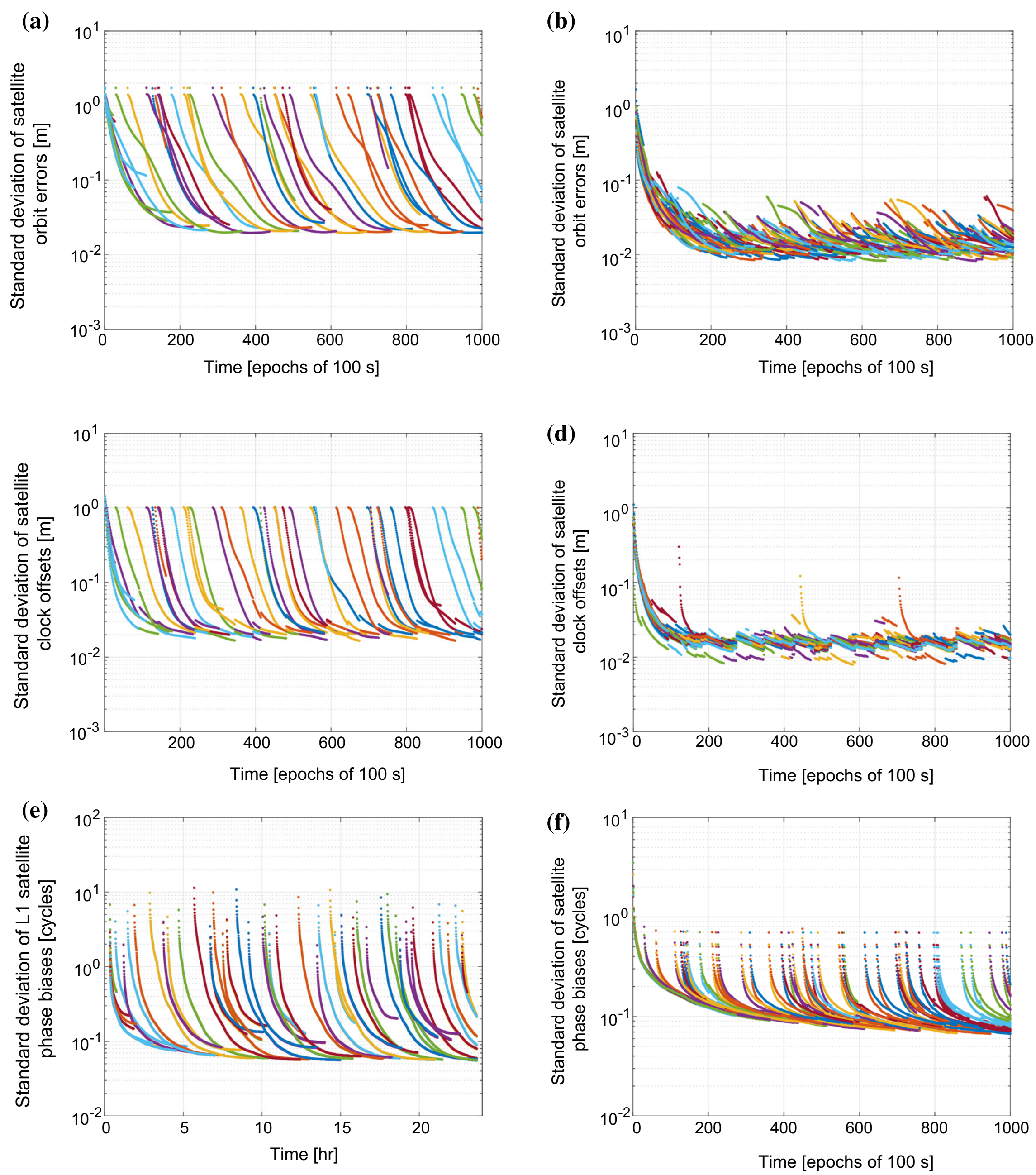

Fig. 8 Benefit in precision of multi-cluster estimation of satellite position corrections, satellite clock offsets and phase biases with **float** ambiguities. Each colour represents a different satellite. **a** Single-cluster satellite position corrections. **b** Multi-cluster satellite position corrections. **c** Single-cluster satellite clock offsets. **d** Multi-cluster satellite clock offsets. **e** Single-cluster satellite phase biases. **f** Multi-cluster satellite phase biases

zenith and ionospheric slant delays and integer ambiguities with real L1/L2 dual-frequency ($M = 2$) GPS measurements with a sampling rate of 30 s. The day of year (DOY) 150 in the year 2017 was selected due to the high availability of data and average ionospheric conditions.

In case of active ionospheric conditions, the measurement and process noise statistics would need to be adjusted since the phase noise is increased during ionospheric scintillations and the temporal variability of the ionospheric delay is larger. We used 77 Multi-GNSS Experiment (MGEX) stations described in Montenbruck et al. (2016) and defined 11 clusters as shown in Fig. 10. Obviously, the number of receivers per cluster is lower than in the simulations since the data of some stations were not used due to outliers. The

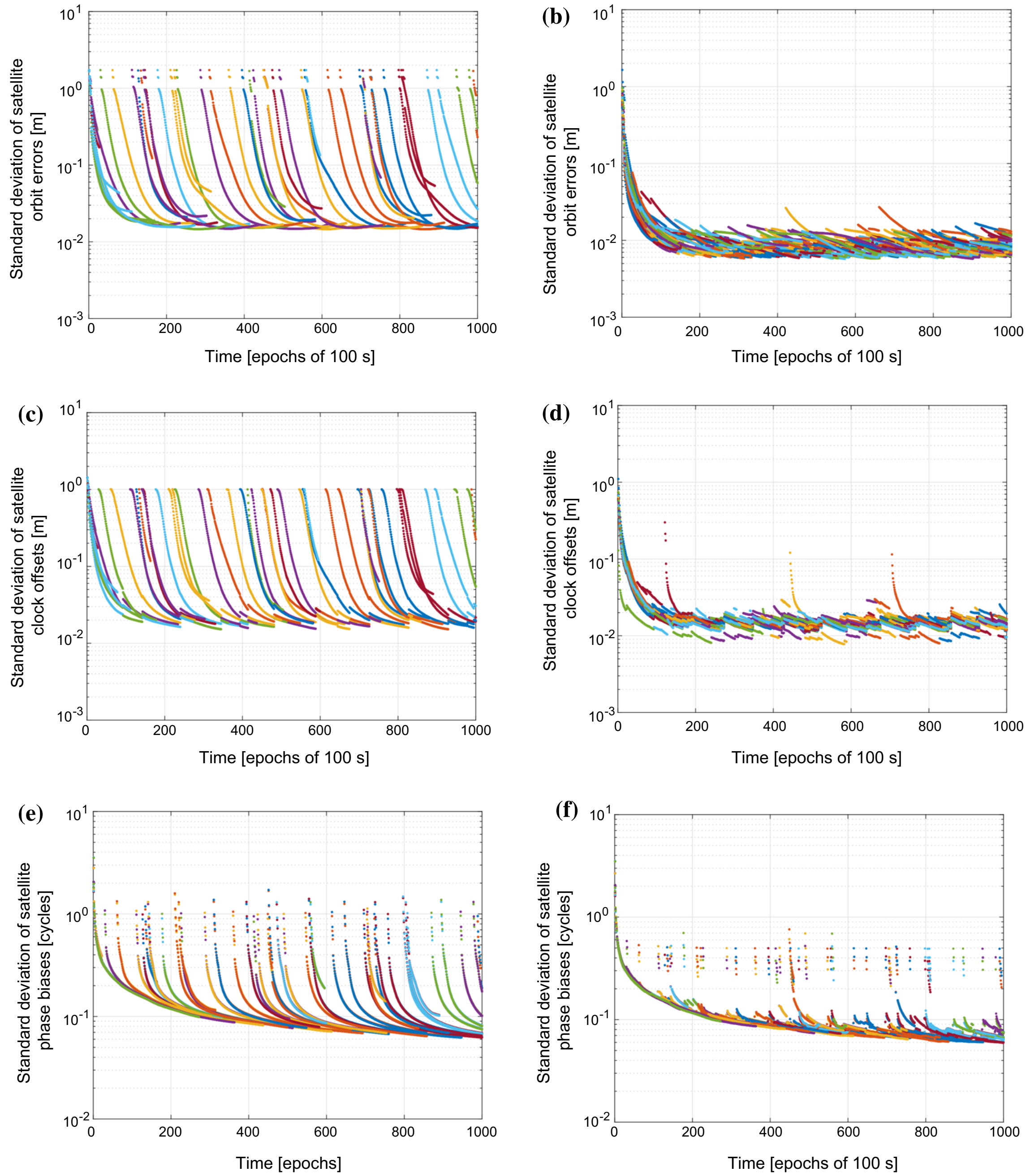

Fig. 9 Benefit in precision of multi-cluster estimation of satellite positions corrections, satellite clock offsets and phase biases with **fixed** ambiguities. Each colour represents a different satellite. **a** Single-cluster satellite position corrections. **b** Multi-cluster satellite position corrections. **c** Single-cluster satellite clock offsets. **d** Multi-cluster satellite clock offsets. **e** Single-cluster satellite phase biases. **f** Multi-cluster satellite phase biases

number of receivers per cluster is provided in the upper left corner of each cluster.

The reference cluster and the reference receiver of each cluster are additionally highlighted. The ambiguities were treated as float numbers as the number of receivers per cluster was too small for reliable ambiguity fixing. Nevertheless, the time constancy of ambiguities was taken into account by setting the process noise of ambiguities to zero.

A pre-processing was performed to eliminate outliers, to correct for cycle slips and to estimate the measurement noise statistics. The process noise statistics were modelled according to Table 2, whereas we have used similar values

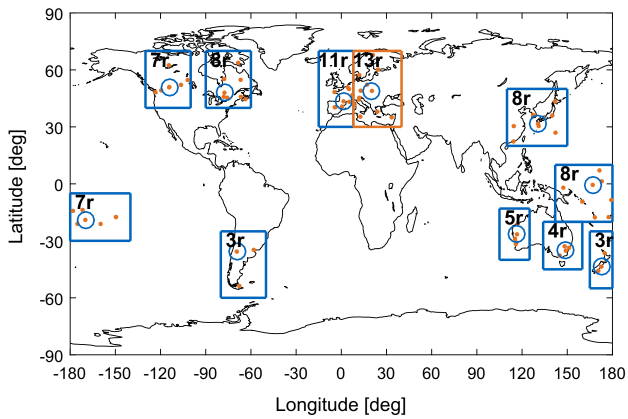

Fig. 10 IGS Multi-GNSS network with 11 clusters: the number of receivers per cluster is provided in the upper left corner of each cluster. The reference receiver of each cluster and the reference cluster are additionally highlighted

Table 2 Process noise statistics and accuracy of prior information

State parameters	σ_x	$\sigma_{\bar{x}}$
Satellite position corrections	0.02 m	1.0 m
Receiver clock offsets	1 km	–
Satellite clock offset corrections	1 m	1.5 m
Tropospheric zenith delays	0.002 m	–
Ionospheric slant delays	0.02 m	–
Receiver phase biases	0.001 m	–
Satellite phase biases	0.001 m	–
Integer ambiguities	0	–

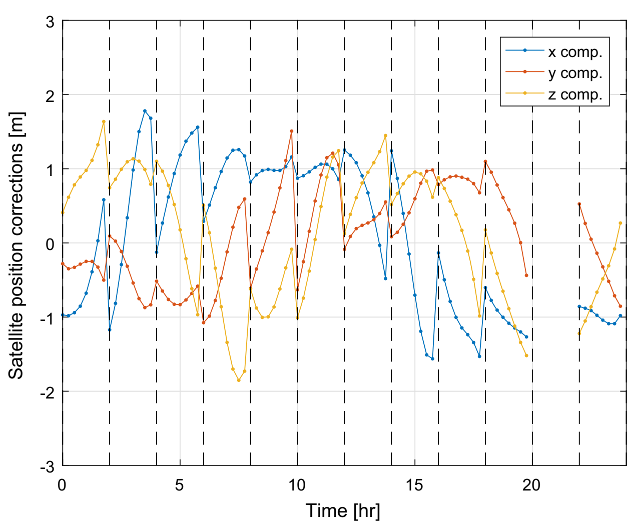

Fig. 11 Satellite position corrections for broadcast orbit of PRN 1 on DOY 150 in 2017

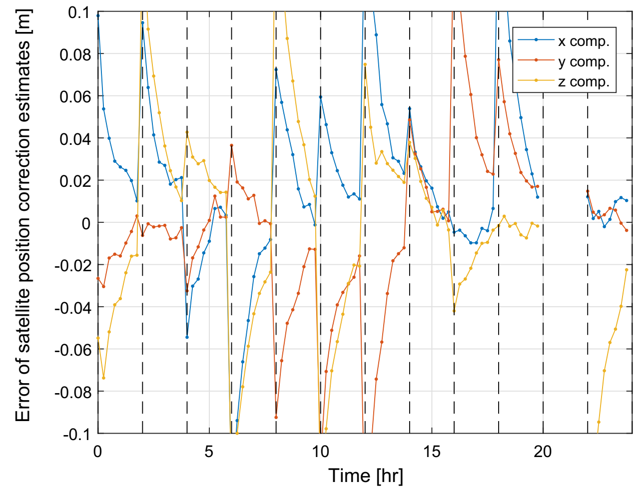

Fig. 12 Deviation between estimated satellite position and IGS orbit based satellite position for PRN 1 on DOY 150 in 2017

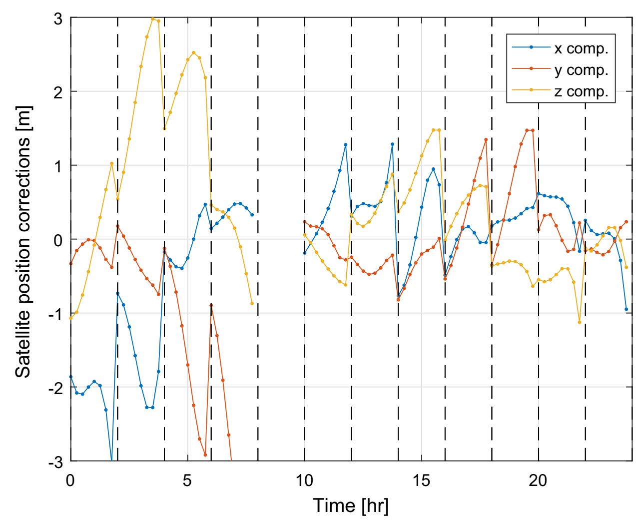

Fig. 13 Satellite position corrections for broadcast orbit of PRN 2 on DOY 150 in 2017

to Laurichesse et al. (2010) and Hauschild and Montenbruck (2009).

Figure 11 shows the obtained satellite position correction estimates for the broadcast orbit of PRN 1. The corrections show a jump every 2 hours due to the updates of the broadcast orbits and a smooth trajectory in between the updates. The accuracy of the estimated satellite corrections and, thereby, of the satellite positions can be obtained by a comparison with the IGS orbits. Figure 12 shows the deviation between our estimated satellite position and the IGS orbits. We can observe that that the error converges from decimetre level to a few centimetres within every 2-h cycle.

A similar picture is obtained for the other satellites, e.g. the satellite position corrections of PRN 2 and their accuracy are provided in Figs. 13 and 14.

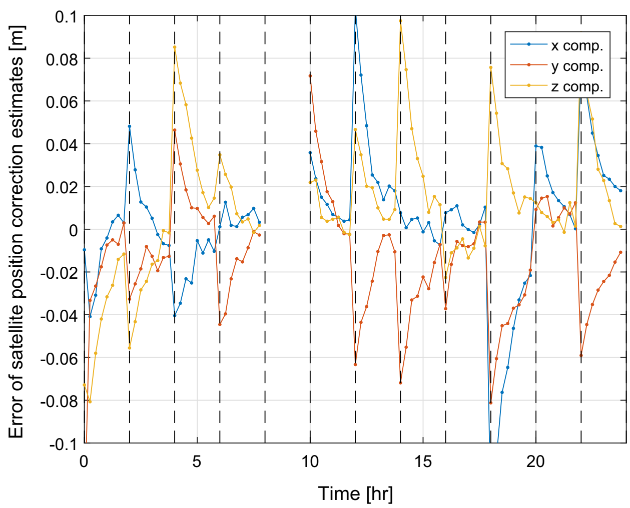

Fig. 14 Deviation between estimated satellite position and IGS orbit based satellite position for PRN 2 on DOY 150 in 2017

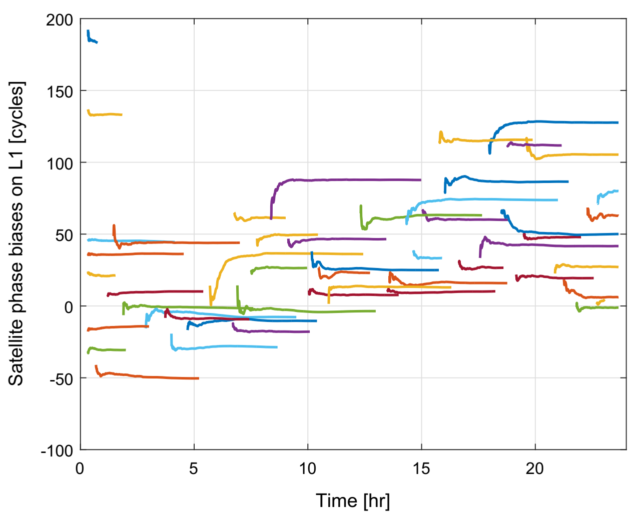

Fig. 15 Satellite phase bias estimates (including mapped phase bias and ambiguity of cluster's reference receiver) on L1 with float ambiguities on DOY 150/2017, derived from the Western European cluster solution. Each colour represents a different satellite

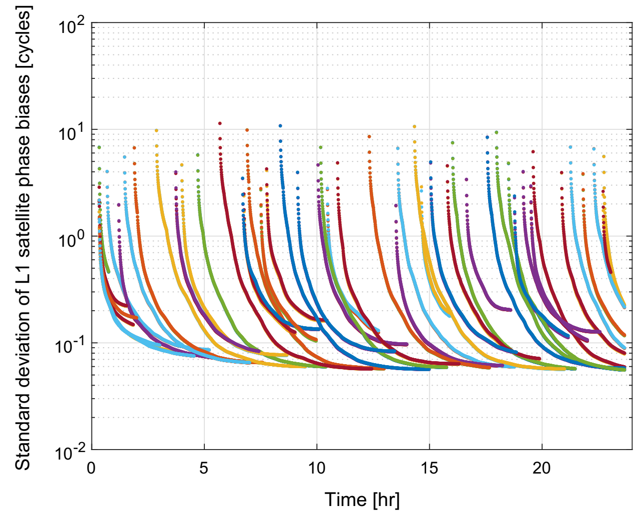

Fig. 16 Standard deviation of satellite phase bias estimates on L1 with float ambiguities on DOY 150/2017, derived from the Western European cluster solution. Each colour represents a different satellite

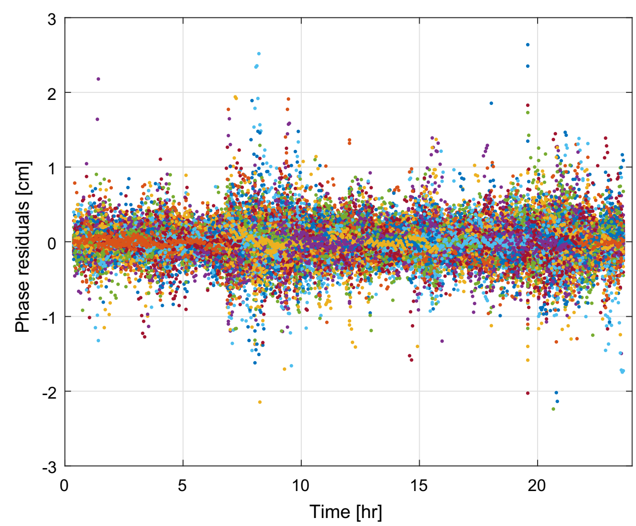

Fig. 17 Phase measurement residuals on DOY 150/2017, derived from the Western European cluster solution. Each colour represents a different measurement

The estimated satellite clock offsets cannot be compared directly with IGS due to the different parameter mapping given by Eqs. (14) and (35). However, the S-transformation of Baarda (1973) could be used to compare the satellite clock offsets on a between-satellite single-differenced form. The further analysis focuses on the satellite phase bias corrections.

Figure 15 shows the estimates of the L1 satellite phase biases of Eq. (17) of the *single*-cluster solution of the Western European cluster for float ambiguities. It has to be noted that the absolute value of the satellite phase biases is irrelevant, as the phase bias and ambiguity of the reference receiver are mapped to the absolute satellite phase biases. The stability of the bias corrections is more relevant as fast fluctuations would require frequent bias updates for the precise point positioning user of the corrections. However, we can observe a stable behaviour for the phase bias estimates of almost all satellites after initial convergence. The convergence time ranges from a few to several hours. Therefore, the phase bias estimates referring to satellites being observed only for a short amount of time do not converge sufficiently.

Figure 16 illustrates the achieved precision of the L1 satellite phase bias estimates in terms of the formal standard deviation as provided by the Kalman filter in the state update. The convergence time for satellite phase bias estimates of newly tracked satellites is in the order of 3 hours. A precision

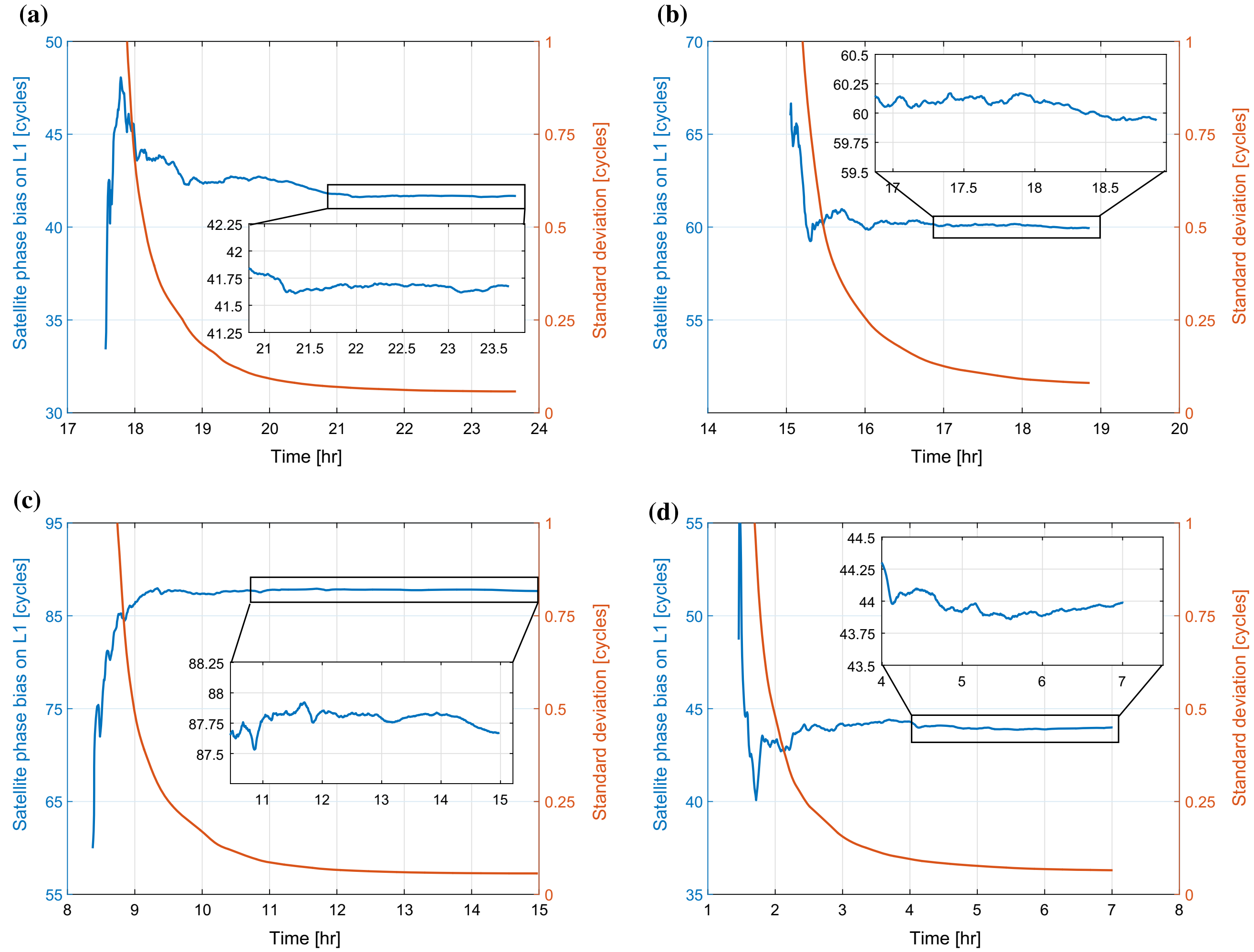

Fig. 18 Satellite phase bias estimates on L1 (including mapped phase bias and ambiguity of cluster's reference receiver) along with their standard deviations for four representative GPS satellites on DOY 150/2017, derived from the Western European cluster solution. **a** PRN11. **b** PRN18. **c** PRN25. **d** PRN30

between 0.05 and 0.20 cycles, or 1 and 4 cm, respectively, is achieved after initial convergence.

Figure 17 shows the phase measurement residuals for DOY 150/2017, derived again from the Western European single- cluster solution. The residuals are an indicator for the quality of the measurement model and the used observations, since the former include the measurement noise, multipath and other unmodelled effects. The phase residuals do not exceed the level of 3 cm and remain even below 1 cm for 99.7% of the time, which confirms the high quality of the selected data.

Figure 18 presents a more precise picture of the satellite phase bias estimates by depicting the L1 satellite phase biases of four representative GPS satellites, plus their formal standard deviations. It can be clearly seen that the satellite phase biases show a high stability with variations between 2 and 5 cm per hour during a satellite's pass after convergence. An hour or even less is sufficient for the bias estimates to converge to an almost constant value. It has to be noted that the absolute value of the satellite phase biases is irrelevant, as the phase bias and ambiguity of the reference receiver are mapped to the absolute satellite phase biases. The formal precision of the satellite phase biases on L1 reaches the 0.10 cycles (∼ 2 cm) level after 2 hours, while the stable level of 0.05 cycles (∼ 1 cm) is achieved after about 5 hours.

Figure 19 shows the *widelane* (L1–L2) satellite phase bias estimates obtained by differencing the satellite phase bias estimates on frequencies L1 and L2. The errors of the satellite phase bias estimates on frequencies L1 and L2 are highly correlated and mostly drop by differencing. Therefore, the widelane phase bias estimates show an even higher stability over time than the uncombined satellite phase bias estimates on L1 and L2.

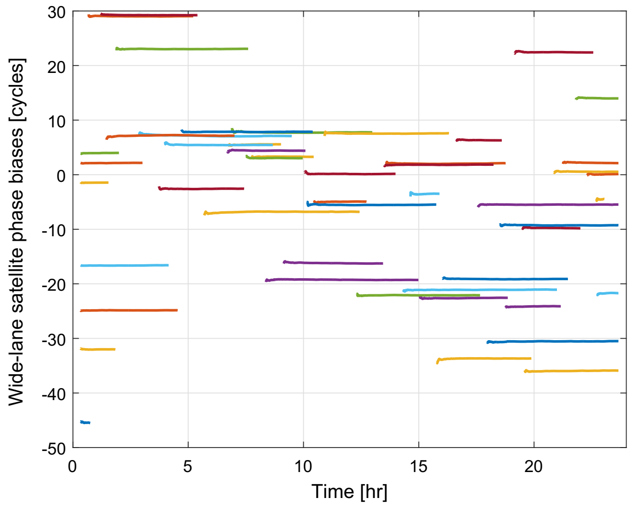

Fig. 19 Widelane satellite phase bias estimates (including mapped phase bias and ambiguity of cluster's reference receiver) with float ambiguities on DOY 150/2017, derived from the Western European cluster solution. Each colour represents a different satellite

10 Conclusion

In this paper, we presented a method for the estimation of satellite position, clock and phase bias corrections, tropospheric zenith and ionospheric slant delays, and integer ambiguities with a global network of reference stations. Undifferenced and uncombined measurements of an arbitrary number of frequencies can be processed such that the obtained corrections can be used for precise point positioning with any type of differenced or combined measurements. The method uses a parameter mapping that leads to a full-rank system and maintains the integer property of ambiguities for a maximum number of ambiguities. We derive this mapping from a global perspective.

The method splits the global network into multiple clusters and selects a reference receiver and reference satellite within each cluster as well as one reference cluster among all clusters. The clustering enables a common satellite visibility within each cluster and, thus, the exploitation of the integer property of double- difference ambiguities. We set up a Kalman filter for each cluster to estimate the satellite position, clock and phase bias corrections, atmospheric delays and ambiguities. An integer decorrelation and sequential adjustment are used to fix the double- difference ambiguities within each cluster and to adjust all other state parameters, respectively. Subsequently, the satellite position, clock and phase bias corrections of each cluster are combined into a global multi-cluster solution by least-squares estimation. Finally, an integer decorrelation and sequential adjustment are used again to fix the double difference ambiguities related to reference stations of different clusters and to readjust the other state parameters.

The proposed method is validated with both simulated Galileo measurements and real GPS measurements from the global IGS network. The ambiguities were fixed to integers for simulated measurements and kept float-valued for real measurements due to the sparsity of the used reference stations. We obtain satellite position, clock and phase bias corrections with an accuracy of better than 2 cm for the simulated Galileo measurements and a precision of 2 cm for the real GPS measurements.

Acknowledgements The authors would like to thank the International GNSS Service (IGS) [see Dow et al. (2009)] for providing the GNSS measurements and the orbital reference of this work.

References

Baarda W (1973) S-transformations and criterion matrices. Publ Geodesy 5(1):18

Blewitt G (1989) Carrier phase ambiguity resolution for the global positioning system applied to geodetic baselines up to 2000 km. J Geophys Res 94(B8):10187–10203

Brack A, Henkel P, Günther C (2014) Sequential best integer equivariant estimation for GNSS. Navigation 61(2):149–158

Brown RG, Hwang PYC (2012) Introduction to random signals and applied Kalman filtering, 4th edn. Wiley, New York

Bryson AE, Henrikson LJ (1968) Estimation using sampled data containing sequentially correlated noise. J Spacecr Rockets 5(6):662–665

Collins P (2008) Isolating and estimating undifferenced GPS integer ambiguities. In: Proceedings of ION NTM, ION, San Diego, CA, USA, pp 720–732

Collins P, Bisnath S, Lahaye F, Héroux P (2010) Undifferenced GPS ambiguity resolution using the decoupled clock model and ambiguity datum fixing. Navigation 57(2):123–135

Dach R, Hugentobler U, Fridez P, Meindl M (2007) Bernese GPS Software Version 5.0, User manual. Astronomical Institute, University of Bern, Switzerland

Dong D, Bock Y (1989) Global positioning system network analysis with phase ambiguity resolution applied to crustal deformation studies in California. J Geophys Res 94:3949–3966

Dow JM, Neilan RE, Rizos C (2009) The international GNSS service in a changing landscape of global navigation satellite systems. J Geodesy 83(3):191–198

Elsobeiey M, Al-Harbi S (2016) Performance of real-time precise point positioning using IGS real-time service. GPS Solut 20(3):565–571

Gabor M, Nerem R (2002) Satellite–satellite single-difference phase bias calibration as applied to ambiguity resolution. Navigation 49(4):223–242

Ge M, Gendt G, Rothacher M, Shi C, Liu J (2008) Resolution of GPS carrier-phase ambiguities in precise point positioning (PPP) with daily observations. J Geodesy 82:389–399

Geng J, Bock YD (2013) Triple-frequency GPS precise point positioning with rapid ambiguity resolution. J Geodesy 87:449–460

Hauschild A, Montenbruck O (2009) Kalman-filter-based GPS clock estimation for near real-time positioning. GPS Solut 13:173–182

Henkel P, Günther C (2010) Partial integer decorrelation: optimum trade-off between variance reduction and bias amplification. J Geodesy 84(1):51–63

Henkel P, Mittmann U, Iafrancesco M (2016) Real-time kinematic positioning with GPS and GLONASS. In: Proceedings of 24th Euro-

pean signal processing conference (EUSIPCO), IEEE, Budapest, Hungary, pp 1–5
Kouba J, Héroux P (2001) GPS precise point positioning using IGS orbit products. GPS Solut 5:12–28
Laurichesse D, Mercier F (2007) Integer ambiguity resolution on undifferenced GPS phase measurements and its application to PPP. In: Proceedings of 20th ION GNSS, ION, Fort Worth, TX, USA, pp 839–848
Laurichesse D, Mercier F, Berthias JP, Broca P, Cerri L (2009) Integer Ambiguity resolution on undifferenced GPS phase measurements and its application to PPP and Satellite precise orbit determination. Navigation 56(2):135–149
Laurichesse D, Mercier F, Berthias JP (2010) Real-time PPP with undifferenced integer ambiguity resolution, experimental results. In: Proceedings of 23rd ION GNSS, ION, Portland, Oregon, USA, pp 2534–2544
Lindlohr W, Wells D (1985) GPS design using undifferenced carrier beat phase observations. Manuscr Geod 10:255–295
Montenbruck O, Steigenberger P, Prange L, Deng Z, Zhao Q, Perosanz F, Romero I, Noll C, Stürze A, Weber G, Schmid R, MacLeod K, Schaer S (2016) The multi-GNSS experiment (MGEX) of the international GNSS service (IGS)—achievements, prospects and challenges. Adv Space Res 59(7):1671–1697
Odijk D, Zhang B, Khodabandeh A, Odolinski R, Teunissen P (2016) On the estimability of parameters in undifferenced, uncombined GNSS network and PPP-RTK user models by means of S-system theory. J Geodesy 90:15–44
Seepersad G, Banville S, Collins P, Bisnath S, Lahaye F (2016) Integer satellite clock combination for precise point positioning with ambiguity resolution. In: Proceedings of 29th ION GNSS, ION, Portland, OR, USA, pp 2058–2068
Teunissen PJG (1995) The least-squares ambiguity decorrelation adjustment: a method for fast GPS ambiguity estimation. J Geodesy 70:65–82
Teunissen PJG (1998) Success probability of integer GPS ambiguity rounding and bootstrapping. J Geodesy 72:606–612
Wen Z, Henkel P, Günther C (2011) Reliable estimation of phase biases of GPS satellites with a local reference network. In: Proceedings of 53rd international IEEE symposium on ELMAR, IEEE, Zadar, Croatia, pp 321–324
Zumberge JF, Heflin MB, Jefferson DC, Watkins MM, Webb FH (1997) Precise point positioning for the efficient and robust analysis of GPS data from large networks. J Geophys Res 102:5005–5017